UNIVERSITY OF LEEDS

This is a repository copy of *Permian−Middle Triassic floral succession in North China and implications for the great transition of continental ecosystems*.

White Rose Research Online URL for this paper:
https://eprints.whiterose.ac.uk/229053/

Version: Accepted Version

Article:
Shu, W., Tong, J., Yu, J. et al. (9 more authors) (2022) Permian−Middle Triassic floral succession in North China and implications for the great transition of continental ecosystems. Geological Society of America Bulletin, 135 (7-8). pp. 1747-1767. ISSN 0016-7606

https://doi.org/10.1130/b36316.1

This item is protected by copyright. This is an author produced version of an article published in GSA Bulletin. Uploaded in accordance with the publisher's self-archiving policy.

Reuse
Items deposited in White Rose Research Online are protected by copyright, with all rights reserved unless indicated otherwise. They may be downloaded and/or printed for private study, or other acts as permitted by national copyright laws. The publisher or other rights holders may allow further reproduction and re-use of the full text version. This is indicated by the licence information on the White Rose Research Online record for the item.

Takedown
If you consider content in White Rose Research Online to be in breach of UK law, please notify us by emailing eprints@whiterose.ac.uk including the URL of the record and the reason for the withdrawal request.

White Rose university consortium
Universities of Leeds, Sheffield & York

eprints@whiterose.ac.uk
https://eprints.whiterose.ac.uk/

Permian–Middle Triassic floral succession in North China and implications for the great transition of continental ecosystems

Wenchao Shu[1], Jinnan Tong[1,*], Jianxin Yu[1,*], Jason Hilton[2], Michael J. Benton[3], Xiao Shi[4], José B. Diez[5], Paul B. Wignall[6], Daoliang Chu[1], Li Tian[1], Zhixing Yi[1], and Yongdong Mao[7]

[1]*State Key Laboratory of Biogeology and Environmental Geology, School of Earth Sciences, China University of Geosciences, Wuhan 430074, China*

[2]*School of Geography, Earth and Environmental Sciences and Birmingham, Institute of Forest Research, The University of Birmingham, Edgbaston, Birmingham B15 2TT, UK*

[3]*School of Earth Sciences, Life Sciences Building, University of Bristol, Bristol, BS8 1TQ, UK*

[4]*School of Earth Sciences, Jilin University, Changchun 130061, China*

[5]*Departamento de Xeociencias Mariñas e Ordenación do Territorio, Facultade de Ciencias do Mar, Universidade de Vigo, Vigo 36310, Spain*

[6]*School of Earth and Environment, University of Leeds, Leeds LS2 9JT, UK*

[7]*Shanxi Institute of Geological Survey, Taiyuan 030006, China*

*Corresponding author. Emails: jntong@cug.edu.cn; yujianxin@cug.edu.cn.

ABSTRACT

The global pattern of plant evolution through the Permian–Triassic mass extinction is uncertain, and the extent to which land plants were affected is debated. Detailed studies undertaken at a regional scale can help evaluate this floral transition, and thus

we provide a detailed account of floral evolution from the Permian to Middle Triassic of North China based on new paleobotanical data and a refined biostratigraphy. Five floral transition events are identified from before, during and after the Permian–Triassic crisis, including the disappearance of the gigantopterid flora (associated with loss of coal deposits), the end-Permian mass extinction of Paleophytic taxa, and gradual recovery in the Triassic with stepwise appearance of the Mesophytic vegetation. The record begins with a Cisuralian gigantopterid-dominated rainforest community, and then a Lopingian walchian Voltziales conifer–ginkgophyte community that evolved into a voltzialean conifer-pteridosperm forest community. The last is associated with a change amongst terrestrial vertebrates from the Jiyuan fauna to a pareiasaur-dominated fauna, found in red beds that lack coal deposits due to arid conditions. The disappearance of the voltzialean conifer forest community may represents the end-Permian mass extinction of plants although it could also be a consequence of the non-preservation of plants in sedimentary red-beds. The first post-crisis plants are an Induan herbaceous lycopsid community, succeeded by the *Pleuromeia-Neocalamites* shrub marsh community. A pteridosperm shrub woodland community dominated for a short time in the late Early Triassic along with the reappearance of insect herbivory. Finally, in the Middle Triassic, gymnosperm forest communities gradually rose to dominance in both uplands and lowlands along with other diverse plant communities, indicating the establishment of the Mesophytic Flora.

Keywords: Permian–Triassic, floral changeover, Paleophytic–Mesophytic transition, continental ecosystem, North China

INTRODUCTION

The response of plant communities to the Permian–Triassic mass extinctions is much debated (e.g. Cascales-Miñana et al., 2016; Nowak et al., 2019). There is no doubt that global floras changed substantially during the Permian–Triassic transition, from the Paleophytic Flora of the late Paleozoic to the Mesophytic Flora of the Mesozoic (Niklas et al., 1983; Cleal and Cascales-Miñana, 2014), but details of the timing are uncertain because of the absence of a robust stratigraphic framework in many terrestrial sections. Regional-scale paleobotanical and palynological work has suggested variable responses to the crisis. Palynological data from East Greenland initially suggested a significant change amongst land plants, especially the disappearance of conifers, followed by delayed recovery (Looy et al., 1999, 2001). Other studies have suggested that there is no extinction in palynological records around the Permian–Triassic Boundary (Hochuli et al., 2016; Schneebeli-Hermann et al., 2017). In Australia and South Africa, a clear extinction is marked by the disappearance of the *Glossopteris* flora (Fielding et al., 2019; Vajda et al., 2020; Mays et al., 2020; Gastaldo et al., 2020; McLoughlin et al., 2021). Data from South China show a considerable loss of land plants during the Permian–Triassic mass extinction (Xiong and Wang, 2011; Yu et al., 2015; Feng et al., 2020; Chu et al., 2020). The changes of macro-plant fossil assemblages from the Permian to Triassic of North China is clear (Wang, 1993; Wang, 2010; Stevens et al., 2011; Lu et al., 2020) but its link with the crisis is uncertain.

The Permian–Triassic mass extinction (252 Ma) was the most severe biotic crisis in the Phanerozoic, and was associated with highly-stressed conditions due to a combination of proposed factors such as global warming (Sun et al., 2012; Benton, 2018; Frank et al., 2021), acid rain (Sephton et al., 2015), wildfires (Shen et al., 2011;

Chu et al., 2020), increased UV-B flux (Visscher et al., 2004; Foster and Afonin, 2005), atmospheric heavy metal pollution (Hochuli et al., 2017), increase of continental weathering (Song et al., 2015; Lu et al. 2020) and strong volcanic activity (Wignall, 2015; Benton, 2018). The crisis eliminated over 80% of marine species, 70% of terrestrial vertebrate species and more than 50% of plant genera, including 42% of lycophytes and ferns, and 70% of gymnosperms, and was followed by the Early Triassic coal gap (Niklas et al., 1983; Retallack et al., 1996; Rees, 2002; Benton, 2014; Cascales–Miñana et al., 2016; Stanley, 2016; Dal Corso et al., 2022).

Here we present an investigation of some groups of continental organisms using a recently refined age model for the Permian to Middle Triassic in North China. Five successive floras are established in association with corresponding vertebrate and invertebrate faunas, which record substantial changes in continental ecosystems during the Paleophytic–Mesophytic transition.

GEOLOGICAL SETTING

During the Permian, six paleofloras were developed in different paleophytogeographical provinces (Chaloner and Lacey, 1973; McLoughlin, 2001, 2011), but during the Early Triassic, provincialism was reduced and a more cosmopolitan lycopsid flora occurred over most of the Northern Hemisphere, while *Dicroidium* forests and locally abundant isoetalean and pleuromeian lycopsids covered the Southern Hemisphere (Fig. 1A). North China, with its Permian Cathaysian Flora, traversed low latitudes (about 30°N), drifting north towards the north-eastern part of the Paleo-Tethys Ocean during the late Paleozoic and early Mesozoic (Fig 1A; Wang et al., 1998). Sedimentary sequences suggest there was a

large lake, about 1400 km wide, in North China during the Permian–Triassic (Fig 1B, C; Zhu et al., 2007; Liu et al., 2015; Ji et al., 2021, 2022).

The Permian to Middle Triassic succession in North China is divided into the Upper Shihhotse, Sunjiagou, Liujiagou, Heshanggou and Ermaying formations. The Upper Shihhotse Formation is dominated by grayish yellow/green sandstone with varicolored (dark red dominated) mud-siltstone. The Sunjiagou Formation comprises red thin- to medium-bedded mudstones with some red sandstones and interbedded calcareous nodules; the overall association is interpreted as a fluvial and floodplain system (Zhu et al., 2007; Zhu et al., 2020; Ji et al., 2022). Intermittent marine flooding occurred, indicated by some marine fossils in the upper part of the formation in the southwestern part of the study region (Yin and Lin, 1979; Chu et al., 2019). The overlying Liujiagou Formation is composed of massive red sandstones with a few interbedded mud-siltstones, locally bearing wrinkle structures, usually taken as evidence of microbial mats (Chu et al., 2015; Tu et al., 2016). There are mud cracks and ripple marks in the lower part, and some large sand sheets interbedded with thick conglomerates in the middle–upper part. This unit was deposited in various fluvial or lake-shore environments (Zhu et al. 2020; Ji et al. 2022). The Heshanggou Formation consists of red siltstones interbedded with some thin sandstone beds and abundant calcareous nodules, interpreted to have formed in shallow lakes (Hu et al., 2009). The Ermaying Formation comprises grayish green, thick-bedded sandstones with green and red thin-bedded mudstones and was deposited in fluvial-lacustrine settings. Abundant fossil plants and sporomorphs have been identified from various locations (Fig. 1D and Supplementary Data File 1).

The ages of the studied formations have been discussed for a long time, and are derived from isolated fossils, magnetostratigraphy, chemostratigraphy and a few U-Pb

123 dates from ash beds. A recent U-Pb zircon study (Wu et al., 2021) shows that most of
124 the Upper Shihhotse Formation is of latest Asselian to early Kungurian age (294.8 ±
125 1.2–≤ 280.73 ± 0.12 Ma) rather than Guadalupian–early Lopingian as previously
126 thought, although its uppermost part may still be latest Capitanian–Lopingian (≤
127 261.75 ± 0.29 Ma). Most of the Guadalupian seems to be absent in parts of North
128 China in this new dating scheme (Wu et al., 2021) whilst the magnetostratigraphy of
129 the uppermost Upper Shihhotse Formation indicates a Wuchiapingian age (Guo,
130 2022). The negative carbon isotope excursions in organic matter ($\delta^{13}C_{org}$) in the
131 middle part of the Sunjiagou Formation provides a potential marker for a latest
132 Changhsingian age (Wu et al., 2020) and a mixed marine-continental fauna marking
133 the Permian–Triassic transitional beds was identified in the middle–upper part of the
134 Sunjiagou Formation (Chu et al., 2019). A CA-ID-TIMS U-Pb age of 252.21 ± 0.15
135 Ma from the middle part of the Sunjiagou Formation in the Shichuanhe section also
136 suggests a latest Changhsingian age for the middle part of the Sunjiagou Formation
137 (Guo et al., 2022). Thus, the Permian–Triassic boundary (PTB) lies in the upper part
138 of the Sunjiagou Formation according to carbon isotope stratigraphy, biostratigraphy
139 and magnetostratigraphy (Chu et al., 2017; Shu et al., 2018; Guo et al., 2019; Wu et
140 al., 2020; Lu et al., 2020; Guo et al., 2022). The basal beds of the overlying Liujiagou
141 Formation yield the *Aratrisporites-Alisporites* sporomorph assemblage (Ouyang and
142 Zhang, 1982; Ouyang and Wang, 1985), and the lycopsid *Pleuromeia* occurs in the
143 upper part of the Liujiagou Formation (Wang and Wang, 1982), all indicating an
144 Early Triassic age (Wang, 1993; Shu et al., 2018; Guo et al., 2019), as does an LA-
145 ICP-MS age of 251 ± 4 Ma from the middle part of the Liujiagou Formation (Zhu et
146 al., 2019). Magnetostratigraphy suggests the Induan–Olenekian boundary is found in
147 the lower part of the Liujiagou Formation (Guo et al., 2022). The Heshanggou

148 Formation yields abundant trace fossils together with body fossils (e.g., fossil plants,
149 vertebrates, fishes, conchostracans (= diplostracans) and ostracodes) of late Early
150 Triassic age (Wang et al., 1978; Qu et al., 1983; Nesbitt et al., 2011). Moreover,
151 magnetostratigraphy confirms an Olenekian age for the Heshanggou Formation (Guo
152 et al., 2022). An ID-TIMS U-Pb zircon date of 243.528 ± 0.069 Ma dates the upper
153 member of the Ermaying Formation as Anisian (Middle Triassic) (Liu et al., 2018).
154 Magnetostratigraphy indicates the Olenekian–Anisian boundary occurs in the basal
155 Ermaying Formation (Guo et al., 2022).

156 Here, we focus on five Permian–Triassic sections that yield well-preserved fossil
157 plants: the Liulin, Peijiashan, Dayulin, Shichuanhe and Zishiya sections (Fig. 1B, C;
158 Fig. 2). In addition, we also mention some other fossil sites with rich plant fossils,
159 such as Heshun, Pingyao and Yushe in Shanxi Province. In the following account, we
160 first focus on the biotas. The potential taphonomic issues that might bias the results
161 will be detailed in the discussion.

162

163 **MATERIALS AND METHODS**

164 This study is mainly based upon over 1400 plant megafossil specimens collected
165 from eight locations ranging through all the target formations in North China (Table
166 1). These include compression, impression and permineralized fossils. The fossils
167 represent shoots, leaves, cones or fertile parts and some trunks/fossil woods, most of
168 which were identifiable. We also restudied all reported fossils from North China and
169 in total we note 52 genera of vertebrates, 42 genera of invertebrates, 102 genera and
170 some form types of plants from over 120 locations (Supplementary Data Files 1–7). In
171 addition, some well-preserved cuticles were prepared by HF/HCl maceration and
172 Schultze solution for oxidation, and KOH to remove remnant humic acids (Kerp,

1990; Jones and Rowe, 1999). *In situ* pollen from male cones or fertile shoots were processed by HF/HCl maceration (Jones and Rowe, 1999). All fossils studied are stored in the paleontological collection of the State Key Laboratory of Biogeology and Environmental Geology, China University of Geosciences (BGEG, Wuhan).

Plant megafossil specimens were photographed using a Canon EOS 7D digital camera, and some *in situ* pollen, bract-scale complexes, small shoots and conchostracan specimens were examined and photographed using a LEICA-DM-750P microscope equipped with an automatic camera image stacking system. Some photos were processed by focus stacking methods using Photoshop CS5 (auto-align layers and auto-blend layers). Some *in situ* pollen were studied using a Hitachi SU8010 scanning electron microscope. In addition, one tetrapod tooth fossil from the uppermost Upper Shihhotse Formation and one well-preserved strobilus of *Pleuromeia* from the Liujiagou Formation were scanned using a nanoVoxel 4000 micro-computed tomography scanner (Sanying Precision Instruments, Tianjing, China) and the raw projections were converted into image stacks using VoxelStudio Recon (Sanying Precision Instruments). The isometric voxel size (spatial resolution) for the *Pleuromeia* and the tooth were 31.60 μm and 17.63 μm, respectively. To image the inner structure of the tooth, its volume data were segmented using the watershed algorithm in Avizo 8.0, and manual correction was performed to correct defects.

For paleoecological analysis, we normalized genera of fossil plants as binary data, present (1) or absent (0), in each formation (Cleal et al., 2021). The presence-absence matrix was then analyzed in R by hierarchical clustering using the Euclidean complete method, *k*-means clustering and principal components analysis (PCA) (Fig. S3–5). The R code is provided in the Supplementary material. To calculate the hygrophyte(H)/xerophyte(X) ratio, plant genera were classified as hygrophytes,

mesophytes and xerophytes based on previous studies (Supplementary data files 9 and 10) and then the ratio calculated as [H/(H+X)]/[X/(H+X)] (DiMichele et al., 2020; Koll and DiMichele, 2021; Supplementary datafile 10).

MACROFLORAS FROM PERMIAN TO MIDDLE TRIASSIC IN NORTH CHINA

Based on collected specimens and previously reported data, five successive macrofloras were identified from the Permian to Lower Triassic in North China. Previously, most of the floras were named after the formations in which they occurred, but here we consistently refer to them based on the index fossils because some of the floras span more than one formation. The gigantopterid flora in the Upper Shihhotse Formation has been well-studied previously (Wang, 2010; Stevens et al., 2011) and we confirm those earlier results. Here we focus on the other four macrofloras, i.e. the Voltziales flora in the uppermost part of the Upper Shihhotse and the Sunjiagou formations, the *Pleuromeia–Neocalamites* flora in the middle–upper part of the Liujiagou and the base of the Heshanggou formations, the *Pleuromeia–Tongchuanophyllum* flora in the lower–upper part of the Heshanggou and the basal part of the Ermaying formations, and the *Lepacyclotes–Voltzia* flora in the lower to upper parts of the Ermaying Formation.

The Voltziales flora

This flora occurs in the uppermost part of the Upper Shihhotse Formation and the lower part of the Sunjiagou Formation. It is dominated by Voltziales conifers, including walchian and voltzian voltzialean type conifers. Here the Voltziales flora is

222 subdivided into the ginkgophyte–walchian Voltziales and the voltzian Voltziales
223 subfloras.
224
225 **The ginkgophyte–walchian Voltziales subflora**
226 This subflora occurs in the uppermost part of the Upper Shihhotse Formation of
227 the Liulin (Fig. 2; Fig. S1B) and Shichuanhe sections (Fig. 2; Fig. S1C). It is
228 dominated by walchian voltzialean shoots, other vegetative-shoot types of conifers
229 (form type 0, 2 and 5, in Supplementary Data File 2), and includes ginkgophytes
230 (form type 1 and 2, in Supplementary Data File 2), pteridosperms (*Autunia*), putative
231 cycadophytes (*Taeniopteris*) and *Sphenopteris*-type foliage (Fig. 3). Gymnosperms
232 are the main elements in this subflora. In the uppermost Upper Shihhotse Formation
233 of the Liulin section, over 80% of plant fossils are shoots and leaves, whereas seed
234 fossils account for about 20%. Around 85% of the shoot compressions/impressions
235 are assigned to conifers and most of these conifer shoots are walchian Voltziales
236 according to their gross morphology and cuticles (Fig. 3, description in
237 Supplementary Data File 2). Some ginkgophyte leaves and *Taeniopteris* locally co-
238 occur with the conifer shoots. In the uppermost Upper Shihhotse Formation of the
239 Shichuanhe section, 385 specimens were collected and 256 identified. Among these,
240 over 65% are assigned to conifer shoots, about 25% are ginkgophyte leaves, and there
241 are a few *Autunia*-type pteridosperm ovuliferous organs, noeggerathialean leaves and
242 other foliage types. In addition, there are some *in situ* monosaccate pollen associated
243 with walchian voltzialean shoots that are elliptical to circular in polar view (Fig. 3X,
244 Y), showing a monolete suture on the corpus, a punctate or in some cases rugulate
245 surface. These are assigned to *Potonieisporites*. This subflora is named the
246 ginkgophyte–walchian Voltziales subflora, after its two dominant elements.

247

248 **The voltzian Voltziales subflora**

249 This subflora of the Voltziales flora was identified from the lower part of the
250 Sunjiagou Formation in the Liulin (Fig. 2; Fig. S1E), Dayulin (Fig. 2; Fig. S1F) and
251 Zishiya (Fig. 2; Fig. S1G) sections. It is dominated by conifers, including
252 *Pseudovoltzia*-type/ *Ullmannia*-type/ other undefined vegetative shoots with well-
253 preserved cuticles (form type 1–4, description in Supplementary Data File 2),
254 *Pseudovoltzia*-type bract-scale complexes with five-lobed scales (Fig. 4AA), male
255 cones with *in situ* monolete bisaccate pollen of the *Gardenasporites*-type (Fig. 4DD,
256 EE, PP, SS) and seeds, with some pteridosperms, such as *Autunia*-type peltate
257 ovuliferous organs and *Germaropteris*-type vegetative small leaves with well-
258 preserved cuticles (Fig. 4, description in Supplementary Data File 2). Calamite stems
259 occur sporadically as compressions or impressions. In the lower part of the Sunjiagou
260 Formation of the Liulin section, 220 discernible specimens were found, 76% of which
261 are shoots, 11% seeds and 13% fertile parts. Around 96% of the shoot
262 compressions/impressions can be assigned to conifers and 4% to ferns and
263 pteridosperms. In the lower part of the Sunjiagou Formation of the Dayulin section,
264 37 identifiable specimens were collected, all of which are conifer shoot compressions
265 and isolated conifer leaf compressions. In addition, there are over 300 specimens from
266 the lower part of the Sunjiagou Formation of the Zishiya section and 202 of these
267 were identifiable. Of these, shoots comprise about 70%, seeds around 19%, fertile
268 parts (including cones) about 8%, and a few stems about 3%. All shoots and one cone
269 can be assigned to conifers, the other fertile parts to the *Autunia* type, a few stems to
270 *Calamites*, and some dispersed seeds to conifers or pteridosperms. This subflora is
271 named after the dominant element as the voltzian Voltziales subflora.

The *Pleuromeia–Neocalamites* flora

Only a few localities, such as Jiaocheng, Yushe and Heshun in Shanxi, yield these plant fossils. They come from the middle-upper part of the Liujiagou Formation and the base of the Heshanggou Formation (Fig. 2). Most of these plant fossils are strobili, isolated sporophylls and rhizomorphs of *Pleuromeia jiaochengensis* and *Pleuromeia sternbergii* (Figs. 5C–K, 6A–D, M). Numerous fragments of *in situ* stems of *Neocalamites* or *Equisetites* preserved as compressions or casts also occur in both red silty mudstones and gray-green siltstones (Figs. 6E–K). Fragments of strap-shaped leaves with parallel veins are possible gymnosperms. Some fragments of sporophylls with long tips characteristic of *Tomiostrobus* were found at the base of the Heshanggou Formation at Heshun (Fig. 6L). In addition, some broken fronds of *Scolopendrites* (Figs. 5A–B) and some dispersed possible male cones, bract-scale complexes and seeds of voltzialean conifers (Figs. 6N–O) occur in this flora. Potential cycadophytes are identified as *Taeniopteris*. This flora is named after the two dominant elements, *Pleuromeia* and *Neocalamites*. *Pleuromeia* by itself is not diagnostic of an individual flora as its stratigraphic range extends into the overlying *Pleuromeia–Tongchuanophyllum* and *Lepacyclotes–Voltzia* floras (see below).

The *Pleuromeia–Tongchuanophyllum* flora

Abundant fossil plant specimens occur in the lower–upper part of the Heshanggou Formation and the basal part of the Ermaying Formation in the Yushe, Pingyao and Puxian sections in Shanxi. Numerous plant fossils have been previously reported from this interval from many other localities, such as Shouyang, Pingyao, Puxian, Fengfeng, Chengde, Jiyuan, and Yima (Supplementary Data Files 2–3). Most

297 of them are lycophytes, e.g., *Pleuromeia epicharis*, some stems with very small leaf
298 cushions *Mesolepidodendron*, some sporophylls with long tips of *Tomiostrobus* (Figs.
299 7A–D, G, H, J–L), and pteridosperms (up to nine genera, e.g., *Tongchuanophyllum*,
300 *Neoglossopteris*, "*Gangamopteris*", *Glossophyllum*, "*Euryphyllum*", *Scytophyllum*,
301 "*Thinnfeldia*", *Sphenopteris* and *Peltaspermum*) (Figs. 7M–O), and the others are
302 sphenophytes (e.g., *Neolobatannularia*, *Phyllotheca*, *Neocalamites*, *Equisetites*) (Figs.
303 7I), pteridophytes (e.g., *Anomopteris, Scolopendrites, Neuropteridium, Todites*),
304 conifers (*Voltzia*, *Yuccites*, *Willsiostrobus*) (Figs. 7P–Q), and putative cycadophytes
305 (possibly *Cycadocarpidium*) (Supplementary Data File 2, 3). This flora is named after
306 its abundant lycopods, dominated by *Pleuromeia*, and the common occurrence of
307 *Tongchuanophyllum*.
308
309 **The *Lepacyclotes–Voltzia* flora**
310 This flora occurs in the lower to upper parts of the Ermaying Formation where
311 the Mesophytic floral elements gradually appear and become more diverse. However,
312 some lycophyte rhizophores (*Pleuromeia*), some lycophyte sporophylls with short tips
313 (*Lepacyclotes*), *Isoetites*, and sphenophytes (*Neocalamites* and *Equisetites*) remain
314 common but sphenophyte stems became larger than those in the former floras (Fig. 8).
315 Fronds and pinnules of true ferns from the lower to upper parts of the Ermaying
316 Formation were identified as *Anomopteris*, *Cladophlebis*, *Danaeopsis*, *Symopteris*
317 (*Bernoullia*) and *Todites* (Supplementary Data File 2, 3). In addition, there is a diverse
318 flora of pteridosperms (e.g., *Germaropteris*, *Peltaspermum*, *Ptilozamites*,
319 *Glossophyllum*, *Neoglossopteris*, *Scytophyllum*, *Tongchuanophyllum*, "*Thinnfeldia*",
320 *Pachypteris* and *Protoblechnum*), cycadophytes (e.g., *Nilssonia*, *Sinozamites* and
321 *Taeniopteris*), ginkgophytes (e.g., *Baiera*, *Ginkgoites* and *Sphenobaiera*) and conifers

(e.g., *Pagiophyllum*, *Podozamites*, *Voltzia* and *Yuccites*) (Supplementary Data File 2, 3). This flora is named after the common Middle Triassic elements, *Lepacyclotes* and *Voltzia*.

DISCUSSION

Ages of the Lopingian to Middle Triassic macrofloras in North China

The floras of North China can be dated with reference to other fossils such as vertebrates. The ginkgophyte–walchian Voltziales subflora of the uppermost Upper Shihhotse Formation of the Shichuanhe and Liulin sections co-occurs with a vertebrate tooth fossil (Fig. 9A–D) of the Jiyuan fauna (Fig. S2; Xu et al. 2015). The Jiyuan Fauna comprises abundant vertebrate taxa (Supplementary Data file 7; Xu et al. 2015) that are assigned a Wuchiapingian age based on comparisons of the entire tetrapod assemblage to the Ilinskoe Subassemblage of the Sokolki Assemblage in Russia and the *Cistecephalus* Assemblage Zone in South Africa (Liu et al. 2014; Benton 2016). A Wuchiapingian age of the strata is also supported by magnetostratigraphy (Guo, 2022).

Previously a *Ullmannia bronnii–Yuania magnifolia* assemblage was documented by Wang and Wang (1986) from the lower–middle part of the Sunjiagou Formation of North China. Unfortunately, we have not collected any *Yuania* in these strata during our reinvestigation (Supplementary Data file 2–3), thus herein we use the term *Ullmannia–Pseudovoltzia–Germaropteris* assemblage as a replacement name. The *Ullmannia–Pseudovoltzia–Germaropteris* assemblage corresponds to the voltzian Voltziales subflora. This subflora and the corresponding *Lueckisporites virkkiae–Jugasporites schaubergeroides* sporomorph assemblage (Hou and Ouyang, 2000) co-occur with a *Pseudestheria* (Fig. 9H–K) conchostracan assemblage in the Liulin and

Dayulin sections (Figs. 2, 9, S2), which is assigned to the Lopingian (probably Changhsingian). In North China, some pareiasaurs (Wang et al., 2019) and fish fossils (Chondrostei and *Platysomus*) (Wang, 1981) were reported from the Sunjiagou Formation and the laterally equivalent Naobaogou Formation (Liu and Bever, 2018, Fig. S2, Supplementary Data file 7). In addition, the *Darwinula–Panxiania* ostracod assemblage occurs in the middle part of the Sunjiagou Formation (Chu et al., 2015, Fig. S2, Supplementary Data file 5). Further, mixed continental-marine biotas (Fig. 9), comprising conchostracans, plants, insects, marine bivalves and lingulid brachiopods, in the middle part of the Sunjiagou Formation are particularly important for biostratigraphic correlation between continental and marine facies (Chu et al., 2019). All the floral data suggest the Permian–Triassic transitional beds start in the middle part of the Sunjiagou Formation. This is further supported by a CA-ID-TIMS U-Pb age of 252.21 ± 0.15 Ma from the middle part of the Sunjiagou Formation in the Shichuanhe section (Guo et al., 2022).

However, some pareiasaurs were also found from the uppermost part of the Sunjiagou Formation at the Xuecun section, Liulin, Shanxi Province (Wang et al., 2019, Fig. S2, Supplementary Data file 7). Pareiasaurs from the continental sections in Russia and South Africa are not considered to have survived the Permian–Triassic mass extinction (Lee, 1997; Benton, 2016). Meanwhile, abundant microbial-induced sedimentary structures (MISS), such as wrinkle structures, appear in the top part of the Sunjiagou Formation and lower part of the Liujiagou Formation at Dayulin (Yiyang, Henan Province), and are common in post-extinction environments (Chu et al., 2015; Tu et al., 2016), as seen in high southern latitudes (Mays et al., 2021a, b). Consequently, the age of the upper part of the Sunjiagou Formation is unclear. The uncertainty over the age of the top of the Sunjiagou Formation may be because the

372 transition with the overlying Sunjiagou Formation is diachronous. An *Aratrisporites–*
373 *Alisporites* sporomorph assemblage, in which *Aratrisporites* is the most abundant
374 element (13.4%), and *Alisporites* is a sub-dominated element (10.3%), occurs with a
375 few fragmentary fossils of *Dicynodon* in the lower part of the Liujiagou Formation
376 (Ouyang and Zhang, 1982, Fig. S2, Supplementary Data file 7), indicating an earliest
377 Triassic (Induan) age. This conclusion is further supported by magnetostratigraphy
378 that indicates a likely Dienerian age for this level (Guo et al., 2022).

379 In the middle part of the Liujiagou Formation in the Peijiashan section and the
380 base of the Heshanggou Formation in the Shichuanhe, Heshun and Yushe sections,
381 the *Pleuromeia–Neocalamites* flora co-occurs with a conchostracan *Leptolimnadia–*
382 *Paleoleptestheria* assemblage and some Triopsidae (Fig. S2, Supplementary Data file
383 5; Tong et al., 2018). Furthermore, from the lower–middle part of the Qishan
384 Formation (equivalent to the Liujiagou Formation) of the Zishiya section, we found a
385 *Lundbladispora–Cycadopites–Protohaploxypinus* sporomorph assemblage that can be
386 correlated to the *Densoisporites nejburgii–Lunatisporites–Cycadopites* sporomorph
387 assemblage (Qu et al., 1980; Qu et al., 1982; Tong et al., 2018). There are also some
388 bivalves, some ophiurids and the *Leptolimnadia–Paleoleptestheria* conchostracan
389 assemblage in the Qishan Formation (Fig. 9G, R, Supplementary Data file 5; Tong et
390 al., 2018), all of which indicate an early Olenekian age.

391 Subsequently, the lower part of the Heshanggou Formation is characterized by
392 the *Pleuromeia–Tongchuanophyllum* flora that is associated with a few tetrapod
393 fossils (e.g., Capitosauridae) (Wang, 1983) and the *Cornia–Estheriella* conchostracan
394 assemblage (Wang, 1983). Higher up in the middle–upper parts of the Heshanggou
395 Formation and basal Ermaying Formation, sporomorphs are assigned to the
396 *Lundbladispora–Verrucosisporites–Lunatisporites* sporomorph assemblage and occur

along with the macroflora documented above (Qu et al., 1980; Ouyang and Norris, 1988; Tong et al., 2018). The sporomorph assemblage includes a higher proportion of gymnosperm pollen (*Cycadopites* and *Lunatisporites*) (Ouyang and Norris, 1988). In addition, vertebrate fossils (including the lungfish *Ceratodus heshanggouensis*) increase in abundance (Wang, 1983, Supplementary Data file 7). Among invertebrates, abundant conchostracans of the *Magniestheria–Eosolimnadia* assemblage occur, together with abundant ostracod fossils of the *Darwinula triassiana–Darwinula fengfengensis–Darwinula rotundata* assemblage (Supplementary Data file 5, Pang, 1989; Tong et al., 2018). Thus, the age of most of the Heshanggou Formation should be Olenekian, except the uppermost part that hosts the *Shaanbeikannemeyeria* assemblage, which is assigned an Anisian age (Liu, 2018; Fig. S2, Supplementary Data file 7).

Finally, in the Ermaying Formation, the *Lepacyclotes–Voltzia* flora is associated with the *Punctatisporites–Chordasporites* sporomorph assemblage (Tong et al. 2018, Fig. S2, Supplementary Data file 2–3). It co-occurs with abundant vertebrate and invertebrate fossils, i.e., the *Sinokannemeyeria–Parakannemeyeria–Shansiodon* tetrapod assemblage (Liu and Sullivan 2017; Liu et al., 2018, Fig. S2, Supplementary Data file 7), the *Brachyestheria–Xiangxiella* conchostracan assemblage (Tong et al. 2018), and the *Lutkevichinella minuta–Shensinella gaoyadiensis–Darwinula subovaliformis* ostracod assemblage (Tong et al. 2018, Fig. S2, Supplementary Data file 5). This biota indicates an Anisian age.

Permian to Middle Triassic floral changes

The Permian-Triassic mass extinction was the most severe event of the Phanerozoic, affecting both marine and continental organisms (Cascales-Miñana et al.

2016; Dal Corso et al., 2022). However, it has been even debated whether there was a mass extinction of land plants (Fielding et al., 2019; Nowak et al., 2019). In North China, it is well known that Permian lands were occupied by the famous *Gigantopteris* (Cathaysian) flora, which gradually went extinct in the later Permian (Hilton and Cleal, 2007; Wang, 2010; Stevens et al., 2011; Wu et al., 2021). There have been few investigations of paleofloral changes at other intervals through the Permian, Early and Middle Triassic (Wang, 1993, 1996; Wang, 2010; Stevens et al., 2011; Yang et al., 2012). A statistical analysis has been especially lacking. Here, we identify six statistically-distinct floras through this interval (Figs. 10–12), separated by five floral transitions (T1–T5 in Fig. 10). Of these distinct floras, two are similar to each other, and they are regarded as the sub-floras of one flora. These changes may help us to understand the Permian–Triassic transition of the plants on land in North China. In some instances, floral transitions are abrupt and can be well-defined by changes in composition at a particular level (represented by horizontal lines in Figure 10). In other cases, the transitions span a broader time interval which may, in part, be due to low sampling frequency.

The first significant floral transition (T1) is recognized between the gigantopterid and Voltziales floras (Fig. 10, 11B (a)). The gigantopterid flora was characterized by high diversity, including abundant and diverse gigantopterids, arborescent lycophytes, diverse sphenophytes and “filicalean” ferns, abundant ginkgophytes, Noeggerathiales and Cordaitales but with few conifers. During this transition (Fig. 11B, from cluster 1 to cluster 2 and from cluster 2 to cluster 3) there is a decrease or the eventual loss of the dominant/characteristic elements, e.g., gigantopterids (Fig. 10). It is characterized by the disappearance of the Cathaysian flora (Wu et al. 2021) and a switch from the Cisuralian gigantopterid flora to the Lopingian Voltziales flora. This also marks the

447 beginning of the Paleophytic to Mesophytic floral switch, which is a staggered event
448 in our analysis. T1 marked the decline and eventual extirpation (regional extinction)
449 of the gigantopterid flora (61.8% genera lost) and replacement by the incoming
450 Voltziales flora that comprises taxa that ranged through this selective extinction event.
451 The second floral transition (T2) occurs within the Voltziales flora and is
452 manifested as the turnover between the two subfloras (Fig. 10, 11) in which 10 taxa
453 disappear, 2 appear and 11 range through the transition. The ginkgophyte–walchian
454 Voltziales subflora (Fig. 10, 11) is dominated by abundant walchian voltzialean
455 conifers and early ginkgophytes, together with the cycad *Taeniopteris*, some
456 pteridosperms (e.g., *Sphenopteris*, *Autunia*, *Supaia*), sphenophytes (e.g.,
457 *Sphenophyllum*), remaining ferns (e.g., *Pecopteris*), a few Noeggerathiales (e.g.,
458 *Yuania*) and a limited appearance of voltzian voltzialean conifers. Overall, the
459 subflora is dominated by gymnosperms (>90%), rather than ferns, and it fits the broad
460 characteristics of the 'Mesophytic age' (Gothan 1912; DiMichele et al., 2008). It is
461 relatively different from the older gigantopterid-dominated flora in North China. So, it
462 may be correlated with previously reported floras from the Upper Shihhotse
463 Formation, such as the upper part of the *Psygmophyllum* zone (Wang, 1993), the post-
464 changeover 4 flora (Wang, 2010) or the post-uUSF extinction flora (Stevens et al.,
465 2011) (Fig. 10). However, there are some differences in the dominant elements in two
466 subfloras of the Voltziales flora. The voltzian Voltziales subflora (Fig. 10, 11) is
467 dominated by voltzian voltzialean conifers, some pteridosperms, and a few
468 sphenophytes and ferns. The presence of a diverse voltzian Voltziales assemblage
469 with a few walchian Voltziales but no early ginkgophytes is especially noteworthy.
470 The third transition (T3) is more difficult to characterize and interpret as it
471 comprises two stages separated by a broad interval lacking plant megafossils from the

Terrestrial ecological disturbance interval (TED interval) (see Xu et al., 2022). T3 commences with the disappearance of the latest Permian voltzian Voltziales subflora with 10/13 loss in genera across a wide range of plant groups (Figs. 10, 11B (b)). This transition event (T3) can be probably regarded as the end Permian plant extinction (EPPE) (Xu et al., 2022) and the PTB plant mass extinction in North China, but it spans a wide time interval due to low sampling frequency (Fig. 10) and is best evidenced by the incoming Early Triassic flora. However, the duration of the crisis could be affected by poor preservation at this level in the TED interval. The dominantly red beds of mudstone and sandstone floodplain facies of the upper part of the Sunjiagou Formation provide a poor fossil plant record (see DiMichele et al., 2008). Such a scenario is supported by the absence of disaster floral elements such as *Pleuromeia*, which appears at a higher level, in the Liujiagou Formation, and the presence of pareiasaurs in the Sunjiagou Formation (Wang et al., 2019; Supplementary Data file 7) which suggests sufficient vegetation existed to support herbivorous vertebrates. Furthermore, the palynoflora from the basal Liujiagou Formation includes the voltzialean conifer pollen *Triadispora* (see Balme, 1995), suggesting that even though the voltzialean-dominated community disappeared in the megafossil record, the group was still present in the region. Plants from this community may not necessarily have been living in the floodplain depositional settings as conifer pollen is widely distributed (Ouyang and Zhang, 1982).

Following the initial loss of plant diversity in T3, the first megaflora of the Early Triassic, the *Pleuromeia–Neocalamites* flora (Fig. 12), is characterized by abundant *Pleuromeia* (typically *Pleuromeia jiaochengensis*) and common sphenophyte stems (*Neocalamites* and *Equisetites*) along with some pteridophytes and a few voltzian conifers (Fig. 10). We consider the appearance of this megaflora to mark the end of

497 the third transition event (T3) (Fig. 10). An alternative interpretation might be to
498 divide the T3 event as presented here into a separate late Permian extinction event and
499 an earliest Triassic radiation event. While future research is required to fully evaluate
500 floral changes in transition, we consider this scenario less likely as the extinction and
501 radiation appear intricately linked to the environmental perturbations of the TED
502 interval.

503 The fourth floral transition (T4), from the *Pleuromeia–Neocalamites* to
504 *Pleuromeia–Tongchuanophyllum* floras (Figs. 10, 11A), represents a radiation event
505 and short-term increase in gymnosperm diversity after the crisis in North China,
506 characterized by the abrupt rise of pteridosperms and a few cycadophytes and conifers.
507 The diversity of *Pleuromeia* also increased noticeably, whereas sphenophytes and
508 pteridophytes increased only slightly (Fig. 10). This transition spans a wide time
509 interval, probably due to low sampling frequency.

510 Finally, the final floral transition (T5) from the *Pleuromeia–Tongchuanophyllum*
511 to the *Lepacyclotes–Voltzia* floras (Fig. 10, 11B (c)) also spans a broad time interval
512 due to low sampling frequency. In this radiation event many taxa co-occur in the
513 *Pleuromeia–Tongchuanophyllum* and *Lepacyclotes–Voltzia* floras showing they are
514 closely related to each other but are nonetheless distinct (Fig. 11). The latter flora is
515 distinguished by a number of incoming pteridophytes, pteridosperms, cycadophytes,
516 ginkgophytes and conifers. The *Lepacyclotes–Voltzia* flora shows full recovery from
517 the Permian–Triassic crisis in terms of diversity and abundance of nearly all higher
518 taxa, including lycophytes, sphenophytes, pteridophytes, pteridosperms, cycadophytes,
519 ginkgophytes and conifers. Gymnosperms increased, especially ginkgophytes,
520 cycadophytes and conifers, and pteridophytes also diversified as tree ferns and ground
521 ferns (Figs. 10, 11, 12).

During the Lopingian, floral distributions were latitude-dependent (Fig. 1A; Supplementary Data file 8), with four distinct floral provinces: the high-northern-latitude *Cordaites* peat-forming flora of the Angaran province (Davydov et al., 2021; Davydov and Karasev, 2021), the low-middle-northern-latitude voltzian Voltziales–pteridosperm floras (e.g., the voltzian Voltziales subflora in North China; Bourquin et al., 2011; Kustatscher et al., 2012, 2017; Cai et al., 2019), the tropical rainforest or lowland-peat-forming floras (e.g., the *Gigantopteris* flora in South China or the Umm Irna flora in Jordan; Yu et al., 2015; Blomenkemper et al., 2018; Feng et al., 2020) and the high-southern-latitude *Glossopteris* peat-forming flora in Gondwana (Fielding et al., 2019). During the Permian–Triassic mass extinction, floras changed dramatically globally. Early Triassic floras were sporadically distributed but with some widespread taxa (Fig. 1A). Herbaceous or shrub-like lycopsid-dominated floras, mainly *Tomiostrobus* and *Pleuromeia*, were widely distributed in the northern hemisphere (Fig. 1A; Supplementary Data file 8), and the *Lepidopteris*- and *Dicroidium*-dominated flora became established in the southern hemisphere (Fig. 1A; Supplementary Data file 8; Vajda et al. 2020).

Evolution of terrestrial ecosystems from Permian to Middle Triassic in North China

Here we discuss the evolution of the ecosystems on land through the Permian–Triassic transition, based on the fossil records of plants, sporomorphs, tetrapods, fishes, invertebrates and trace fossils from North China. The transition was associated with turbulent environmental changes (Fig. 13), some of which led to biological responses, as highlighted by the hygrophyte/xerophyte ratio that reflects changes in

546 floral composition from wet (hygrophyte) to dry (xerophyte) ecological settings
547 (Supplementary Data file 9–10).

548 The subsidence of the Cisuralian gigantopterid-dominated rainforest
549 communities coincides with the last occurrence of coal deposits and the rise of the
550 Lopingian ginkgophyte–walchian Voltziales forest community (Fig. 12) in North
551 China. Disappearance of the *Gigantopteris* flora in North China represents a regional
552 loss of diversity and an extirpation event because many taxa, but not all, and the
553 *Gigantopteris* flora, persist in South China until the late Changhsingian where they
554 are notable victims of the EPPC (e.g., Yu et al., 2015; Feng et al., 2020, Xu et al.,
555 2022). In the meantime, the Jiyuan Fauna changed into the pareiasaur-dominated
556 fauna whilst insect diversity decreased (Fig. 13, Supplementary Data File 6–7; Xu et
557 al., 2015; Wang et al., 2019). The gradual changeover in the *Gigantopteris* flora
558 indicates increasing aridity, a trend that continues in the Voltziales flora (Fig. 13,
559 Supplementary Data file 9–10). A few insect remains (Fig. 9E) still co-occur with
560 conifers in the top of the Upper Shihhotse and Sunjiagou formations (Fig. 2), and then
561 there is no record of insect fossils from the point of disappearance of the
562 Changhsingian conifer forests to the Middle Triassic in North China (Zheng et al.
563 2018). Both plant macrofossils and sporomorph records in the lower–middle parts of
564 the Sunjiagou Formation were from voltzialean-dominated forests. The
565 hygrophyte/xerophyte ratio indicates that arid or semi-arid conditions prevailed
566 during the deposition of the lower–middle parts of the Sunjiagou Formation (Fig. 13).
567 The mean annual precipitation was calculated, based on the depth to the Bk horizon in
568 paleosols, as 320 ±147 mm/yr (Yu et al. 2022).

569 The disappearance of the voltzian Voltziales-dominated forests (T3; Fig. 12) in
570 the latest Changhsingian, is associated with the appearance of red beds commonly and

571 MISS in lacustrine facies (Chu et al. 2015). However, despite the apparent forest
572 floral crisis of the EPPC, some tetrapods persisted in the Upper Sunjiagou Formation
573 (Fig. 2, Liulin section; Fig. 13) as did aquatic invertebrates, such as the
574 conchostracans *Palaeolimnadia* and *Euestheria* and ostracods *Darwinula* and
575 *Panxiania* (Fig. 13, Supplementary Data File 5, 7, Chu et al., 2015). The Voltziales-
576 dominated flora may have persisted in the latest Changhsingian, at the same time as
577 the tetrapod losses, but poor preservation could have "back-smeared" the final
578 occurrence.

579 The Early Triassic (Induan?) *Aratrisporites–Alisporites* sporomorph assemblage
580 (Ouyang and Zhang, 1982) may represent the first herbaceous lycopsid plant
581 community occupying lowlands, coexisting with a few upland gymnosperms (Fig. 12),
582 established after the crisis. This was followed by the early Olenekian *Pleuromeia–*
583 *Neocalamites* flora representing *Pleuromeia*/*Neocalamites*-dominated shrub marshes
584 in muddy wetlands. These occur *in situ* in sandstones or silty mudstones of the
585 Liujiagou Formation and the base of the Heshanggou Formation (Fig. S1H–I),
586 interpreted as braided river and shallow lake environments (Ji et al. 2021).
587 *Pleuromeia*/*Neocalamites*-dominated shrub marshes likely grew in riverbank or
588 muddy floodplain settings. In the late stage of the *Pleuromeia–Neocalamites* flora, a
589 few *Voltzia* conifer shrubs appeared and might have grown in well-drained sandy
590 riverbanks. Some allochthonous fragments of *Tomiostrobus* may have been derived
591 from sporadically distributed plants around small ephemeral water bodies.
592 Concurrently, aquatic invertebrates appeared in this ecosystem, such as
593 conchostracans, ostracods and Triopsidae (Wang, 1983). The hygrophyte/xerophyte
594 ratio indicates a more humid environment in the early Olenekian than during the latest

595 Changhsingian in North China (Fig. 13, Supplementary Data file 9–10), which is
596 consistent with geochemical data from paleosols in North China (Yu et al. 2022).
597 Subsequently, in the *Pleuromeia–Tongchuanophyllum* flora, pteridosperm–
598 conifer shrub woodlands are identified by the appearance of abundant pteridosperms
599 ("*Euryphyllum*", "*Gangamopteris*", *Glossophyllum*, *Neoglossopteris*, *Sphenopteris*,
600 "*Thinnfeldia*", *Tongchuanophyllum*, *Peltaspermum* and *Scytophyllum*) and some
601 *Voltzia* elements (Fig. 12). Lacustrine conditions were predominant in this stage (Hu
602 et al., 2009). These *Voltzia*-dominated woodland communities grew in well-drained
603 sandy-soil riverbanks or other lowlands (Fig. 12). The lycophyte (*Pleuromeia*)–
604 sphenophyte (*Neocalamites*, *Equisetites* and *Phyllotheca*)-dominated shrub marsh
605 community with some pteridophytes (e.g., *Todites*, *Neuropteridium* and *Anomopteris*)
606 was still widely distributed on riverbanks or muddy floodplains (Fig. 12). Some
607 *Tomiostrobus*-dominated, herbaceous, ground-covering communities occurred around
608 the shores of playa lakes. In addition, some insect herbivory damage appeared on
609 leaves of *Tongchuanophyllum* (Fig. 7O), and abundant small, spiral microconchid-like
610 organisms on sporophylls of *Pleuromeia* (Fig. 7D) are preserved. Moreover, many
611 vertebrate fossils (Benthosuchidae, Capitosauridae, Procolophonidae, Scaloposauria,
612 *Eumetabolodon*, *Fugusuchus*, *Hazhenia*, *Pentaedrusaurus* and *Xilousuchus*), some
613 fish (*Ceratodus*) and many invertebrates co-occur with this flora (Wang, 1983,
614 Nesbitt et al., 2011, Fig. 13, Supplementary Data file 7). All these changes suggest
615 that diverse terrestrial and aquatic ecosystems had begun to reappear (Fig. 12). At this
616 time, there are abundant types of trace fossils in continental ecosystems (Fig. 13, Shu
617 et al., 2018; Guo et al., 2019) recording widespread activity on land, as well as
618 posture changes and the evolution of endothermy with insulation (hair, feathers) in
619 synapsid and archosauromorph tetrapods (Benton, 2021). The increase of invertebrate

620 diversity (Fig. 13) may indicate a repopulation of aquatic ecosystems following their
621 disappearance in the late Changxingian. Sporomorphs in the later stages of this flora
622 are represented by the *Cycadopites–Lunatisporites–Verrucosisporites* sporomorph
623 assemblage, and the hygrophyte/xerophyte ratio indicates a relatively seasonally
624 humid environment in the late Olenekian (Fig. 13, Supplementary Data file 9–10) and
625 the mean annual precipitation was calculated to range from 520 ±147 mm/yr to 680
626 ±147 mm/yr (Yu et al., 2022).

627 In the *Lepacyclotes–Voltzia* flora, some xerophytic gymnosperms (e.g.,
628 *Lepidopteris*, *Peltaspermum*, *Pagiophyllum*, *Yuccites* and *Voltzia*) started to occupy
629 some dry uplands (Fig. 12) if they were not already established there; such absences
630 may represent a taphonomic bias towards wetland depositional settings (see
631 Blomenkemper et al., 2018). Along with the increased diversity of pteridophytes,
632 pteridosperms, cycadophytes, ginkgophytes and conifers, the gymnosperm-dominated
633 forest community started to occupy some dry uplands, and the pteridophyte-
634 dominated shrub community entered moist lowlands. The *Pleuromeia*–sphenophyte-
635 dominated shrub marsh community was still on riverbanks or muddy floodplains (Fig.
636 12). At that time, the *Sinokannemeyeria* fauna was widely distributed in North China
637 (Liu and Sullivan, 2017). Aquatic invertebrates probably also increased (Figs. 12, 13),
638 as also suggested by abundant burrows inside the cast of *Neocalamites* (Fig. 8F). The
639 hygrophyte/xerophyte ratio indicates a gradual shift to a more humid climate (Fig. 13,
640 Supplementary Data file 9–10).

641

642 **CONCLUSIONS**

643 A new integrated multifaceted biostratigraphic framework with a refined time
644 scale is established for the Lopingian–Middle Triassic of North China, based on

645 macrofossil plant, sporomorph, vertebrate and invertebrate (conchostracans and
646 ostracodes) assemblages.

647 Five main floras are recognized are identified in North China, the gigantopterid,
648 Voltziales, *Pleuromeia–Neocalamites*, *Pleuromeia–Tongchuanophyllum* and
649 *Lepacyclotes–Voltzia* floras, with the Voltziales flora comprising the ginkgophyte–
650 walchian Voltziales and the voltzian Voltziales subfloras. The five transitions
651 between these floras consist of an extirpation event, two turnover events and two
652 radiation events. The gigantopterid flora regional extinction (T1; 34/55 genera lost)
653 eliminated the gigantopterid-dominated rainforest and saw the end of coal deposition
654 This marks the beginning of the changeover from the Paleophytic to Mesophytic
655 floras. The second floral transition (T2), is a subflora turnover within the Voltziales
656 flora, and saw a change in the dominant elements. The end-Permian plant extinction
657 event (EPPE; T3), which saw the loss of 10 out of 13 genera, marks the start of the
658 terrestrial ecological disturbance interval (TED interval) on land. This crisis was
659 followed by a short-term diversification (T4) from the *Pleuromeia–Neocalamites* to
660 the *Pleuromeia–Tongchuanophyllum* floras. The final floral transition (T5) in the
661 earliest Middle Triassic, indicating the recovery-radiation of plants, represented by the
662 *Lepacyclotes–Voltzia* flora, shows the initial construction of the Mesophytic Flora.

663 From the Cisuralian to Lopingian, the change from a gigantopterid-dominated
664 rainforest community to a voltzialean conifer forest community occurred in parallel
665 with the decline of the Jiyuan fauna and change to a pareiasaur-dominated fauna, loss
666 of coal deposits, sharp increase of red beds and aridity increase. The subsequent
667 disappearance of the voltzialean conifer forest community marks the end-Permian
668 plant extinction in North China. Following the prolonged plant-free Terrestrial
669 ecological disturbance interval the first plants to recover after the crisis belonged to a

herbaceous plant community, followed by a *Pleuromeia–Neocalamites* shrub marsh community. A pteridosperm shrub woodland community dominated for a short time in the late Early Triassic, along with the first appearance of insect herbivory. Finally, in the Middle Triassic, the gymnosperm forest community gradually rose to dominance with the appearance of diverse plant communities on lowland and possible upland settings.

ACKNOWLEDGMENTS

This study was jointly funded by the National Natural Science Foundation of China (grant numbers 9205520023, 42030513, 41661134047 and 41530104) and the UK Natural Environment Research Council's Eco-PT project (NE/P01377224/1) to P.B.W., M.J.B. and J.H. We thank our colleagues, Yuyang Wu, Yingyue Yu, Wenwei Guo, Kaixuan Ji, Xue Miao, Meijia Zhang, Zhen Xu, Xin Sun, Qing Xue, Yuyang Tian and Yan Ye for help in the field and general advice. Especially, we thank Patrick Blomenkemper and Hans Kerp for guidance on cuticular analysis, Jacopo Dal Corso for many constructive suggestions and Weidong Liu of Shanxi Institute of Geological Survey for help with the reference "*Triassic of Shanxi*". We thank the editors Wenjiao Xiao and Ganqing Jiang for their editions and reviews. In addition, we also thank four anonymous reviewers for feedback on the manuscript.

REFERENCES CITED

Balme, B., 1995, Fossil in-situ spores and pollen grains: an annotated catalogue. Review of Palaeobotany and Palynology 87, 81–323.

693 Blomenkemper, P., Kerp, H., Hamad, A.A., DiMichele, W.A., and Bomfleur, B.,
694 2018, A hidden cradle of plant evolution in Permian tropical lowlands. Science, v.
695 362, p. 1414–1416.
696 Benton, M.J., and Newell, A.J., 2014, Impacts of global warming on Permo-Triassic
697 terrestrial ecosystems. Gondwana Research, v. 25, p. 1308–1337.
698 Benton, M.J., 2016, The Chinese pareiasaurs. Zoological Journal of the Linnean
699 Society, v. 177, p. 813–853.
700 Benton M. J., 2018, Hyperthermal-driven mass extinctions: killing models during the
701 Permian–Triassic mass extinction. Philosophical Transactions of the Royal
702 Society A, v. 376, p. 20170076.
703 Benton, M.J., 2021, The origin of endothermy in synapsids and archosaurs and arms
704 races in the Triassic. Gondwana Research, v. 100, p. 261–289.
705 Bourquin, S., Bercovici, A., López–Gómez, J., Diez, J.B., Broutin, J., Ronchi, A.,
706 Durand, M., Arche, A., Linol, B., and Amour, F., 2011, The Permian–Triassic
707 transition and the onset of Mesozoic sedimentation at the northwestern peri–
708 Tethyan domain scale: Palaeogeographic maps and geodynamic implications.
709 Palaeogeography, Palaeoclimatology, Palaeoecology, v. 299, p. 265–280.
710 Broutin, J., Roger, J., Platel, J. –P., Angiolini, L., Baud, A., Bucher, H., Marcoux, J.,
711 and Al Hasmi, H., 1995, The Permian Pangea. Phytogeographic implications of
712 new paleontological discoveries in Oman (Arabian Peninsula). Comptes Rendus
713 de l'Academie des Sciences Paris, Série Iia, v. 321, p. 1069–1086.
714 Broutin, J., Yu, J.X., Shi, X., Shu, W.C. and Qing, X., 2020, Terrestrial palaeofloral
715 succession across the Permian–Triassic Boundary in the North and South China
716 blocks: a brief review. Paläontologische Zeitschrift, v. 94, p. 633–644.

717 Cai, Y.F., Zhang, H., Feng, Z., Cao, C.Q., and Zheng, Q.F., 2019, A *Germaropteris*-
718 dominated flora from the upper Permian of the Dalongkou section, Xinjiang,
719 Northwest China, and its paleoclimatic and paleoenvironmental implications.
720 Review of Palaeobotany and Palynology, v. 266, p. 61–71.
721 Cascales–Miñana, B., Diez, J.B., Gerrienne, P., and Cleal, C.J., 2016, A
722 palaeobotanical perspective on the great end-Permian biotic crisis. Historical
723 Biology, v. 28, p. 1066–1074.
724 Chaloner, W.G., and Lacey, W.A., 1973, The distribution of Late Palaeozoic floras. p.
725 271–290 in Hughes, N.F. Ed., Organisms and continent through time. Special
726 Papers in Palaeontology, v. 12. Palaeontological Association, London.
727 Chu, D.L., Tong, J.N., Song, H.J., Benton, M.J., Bottjer, D.J., Song, H.Y., and Tian,
728 L., 2015, Early Triassic wrinkle structures on land: stressed environments and
729 oases for life. Scientific Reports, v. 5, p. 10109.
730 Chu, D.L., Tong, J.N., Benton, M.J., Yu, J.X. and Huang, Y.F., 2019, Mixed
731 continental–marine biotas following the Permian–Triassic mass extinction in
732 South and North China. Palaeogeography, Palaeoclimatology, Palaeoecology, v.
733 519, p. 95–107.
734 Chu, D.L., Grasby, S.E., Song, H.J., Corso, J.D., Wang, Y., Mather, T.A., Wu, Y.Y.,
735 Song, H.Y., Shu, W.C., Tong, J.N., and Wignall, P.B., 2020, Ecological
736 disturbance in tropical peatlands prior to marine Permian–Triassic mass
737 extinction. Geology, v. 48, p. 288–292.
738 Cleal, C.J., and Cascales-Miñana, B., 2014, Composition and dynamics of the great
739 Phanerozoic Evolutionary Floras. Lethaia, v. 47, p. 469–484.
740 Cleal, C.J., Pardoe, H.S., Berry, C.M., Cascales-Miñana, B., Davis, B.A.S., Diez, J.B.,
741 Filipova-Marinova, M.V., Giesecke, T., Hilton, J., Ivanov, D.A., Kustatscher, E.,

742 Leroy, S.A.G., McElwain, J.C., Opluštil, S., Popa, M.E., Seyfullah, L.J., Stolle,
743 E., Thomas, B.A., and Uhl, D., 2021, Plant diversity in deep time: 1. How well
744 can we identify past plant diversity in the fossil record? Palaeogeography,
745 Palaeoecology, Palaeoclimatology, v. 576, p. 110481.
746 Dal Corso, J., Song, H.J., Callegaro, S., Chu, D.L., Sun, Y.D., Hilton, J., Grasby, S.E.,
747 Joachimski, M.M., Wignall, P.B. 2022. Environmental crises at the Permian–
748 Triassic mass extinction. Nature Reviews Earth and Environment, v. 3, p. 197–
749 214. https://doi.org/10.1038/s43017-021-00259-4
750 Davydov, V.I., Karasev, E.V., Nurgalieva, N.G., Schmitz, M.D., Budnikov, I.V.,
751 Biakov, A.S., Kuzina, D.M., Silantiev, V.V., Urazaeva, M.N., Zharinova, V.V.
752 and Zorina, S.O., 2021, Climate and biotic evolution during the Permian-Triassic
753 transition in the temperate Northern Hemisphere, Kuznetsk Basin, Siberia, Russia.
754 Palaeogeography, Palaeoclimatology, Palaeoecology, v. 573, p. 110432.
755 Davydov, V.I. and Karasev, E.V., 2021, The Influence of the Permian-Triassic
756 Magmatism in the Tunguska Basin, Siberia on the Regional Floristic Biota of the
757 Permian-Triassic Transition in the Region. Frontiers in Earth Science, v. 9, p. 134.
758 DiMichele, W.A., Kerp, H., Tabor, N.J., and Looy, C.V., 2008, The so-called
759 “Paleophytic–Mesophytic” transition in equatorial Pangea — Multiple biomes
760 and vegetational tracking of climate change through geological time.
761 Palaeogeography, Palaeoclimatology, Palaeoecology, v. 268, p. 152–163.
762 DiMichele, W.A., Bashforth, A.R., Falcon-Lang, H.J. and Lucas, S.G., 2020. Uplands,
763 lowlands, and climate: Taphonomic megabiases and the apparent rise of a
764 xeromorphic, drought-tolerant flora during the Pennsylvanian-Permian
765 transition. Palaeogeography, Palaeoclimatology, Palaeoecology, v. 559, art.
766 109965.

767 Feng, Z., Wei, H.-B., Guo, Y., He, X.Y., Sui, Q., Zhou, Y., Liu, H.Y., Gou, X.D., and
768 Lü, Y., 2020, From rainforest to herbland: new insights into land plant responses
769 to the end–Permian mass extinction, Earth–Science Reviews, v. 204, p. 103153.
770 Fielding, C.R., Frank T.D., McLoughlin, S., Vajda, V., Mays, C., Tevyaw, A.P.,
771 Winguth, A., Winguth, C., Nicoll, R.S., Bocking, M., and Crowley, J.L., 2019,
772 Age and pattern of the southern high–latitude continental end–Permian extinction
773 constrained by multiproxy analysis. Nature Communications, v. 10, p. 385.
774 Foster, C.B., and Afonin, S.A., 2005, Abnormal pollen grains: an outcome of
775 deteriorating atmospheric conditions around the Permian–Triassic boundary.
776 Journal of the Geological Society, London, v. 162, p. 653–659.
777 Frank, T.D., Fielding, C.R., Winguth, A.M.E., Savatic, K., Tevyaw, A., Winguth, C.,
778 McLoughlin, S., Vajda, V., Mays, C., Nicoll, R. and Bocking, M., 2021. Pace,
779 magnitude, and nature of terrestrial climate change through the end-Permian
780 extinction in southeastern Gondwana. Geology, v. 49, p.1089–1095.
781 Gall, J. –C., and Grauvogel–Stamm, L., 2005, The early Middle Triassic 'Grès à
782 *Voltzia*' Formation of eastern France: a model of environmental refugium.
783 Comptes Rendus Palevol, v. 4, p. 637–652.
784 Gastaldo, R.A., Kamo, S.L., Neveling, J., Geissman, J.W., Looy, C.V., and Martini,
785 A.M., 2020, The base of the *Lystrosaurus* Assemblage Zone, Karoo Basin,
786 predates the end-Permian marine extinction: Nature Communications, v. 11, art.
787 1428.
788 Gothan, W., 1912, Paläobotanik. In: Korschelt, E., Linck, G., Schaum, K., Simon, H.
789 Th., Verworn, M., Teichmann, E. (Eds.), Handwörterbuch der
790 Naturwissenschaften. Gustav Fischer Verlag, Jena, pp. 408–460 (in German).

791 Guo, W.W., Tong, J.N., Tian, L., Chu, D.L., Bottjer, D.J., Shu, W.C., and Ji, K.X.,
792 2019, Secular variations of ichnofossils from the terrestrial Late Permian–Middle
793 Triassic succession in the Shichuanhe section in Shaanxi Province, North China.
794 Global and Planetary Change, v. 181, p. 102978.
795 Guo, W., Tong, J., He, Q., Hounslow, M.W., Song, H., Dal Corso, J., Wignall, P.B.,
796 Ramezani, J., Tian, L. and Chu, D., 2022. Late Permian–Middle Triassic
797 magnetostratigraphy in North China and its implications for terrestrial-marine
798 correlations. Earth and Planetary Science Letters, v. 585, art. 117519.
799 Guo, W., 2022. Late Permian–Middle Triassic magnetostratigraphic timescale from
800 terrestrial North China and secular variations of ichnofossils. PhD thesis, China
801 University of Geosciences, Wuhan, pp. 228.
802 Hilton, J., and Cleal, C.J., 2007, The relationship between Euramerican and
803 Cathaysian tropical floras in the Late Palaeozoic: palaeobiogeographical and
804 palaeogeographical implications. Earth–Science Reviews, v. 85, p. 85–116.
805 Hochuli, P.A., Sanson-Barrera, A., Schneebeli-Hermann, E. and Bucher, H., 2016.
806 Severest crisis overlooked—Worst disruption of terrestrial environments
807 postdates the Permian–Triassic mass extinction. Scientific Reports, v. 6, art.
808 28372.
809 Hochuli, P.A., Schneebeli–Hermann, E., Mangerud, G., and Bucher, H., 2017,
810 Evidence for atmospheric pollution across the Permian–Triassic transition.
811 Geology, v. 45, p. 1123–1126.
812 Hou, J.P. and S. Ouyang, 2000, Palynoflora from the Sunjiagou Formation in Liulin
813 County, Shanxi Province. Acta Palaeontologica Sinica, v. 39, p. 356–368.

814 Hu, B., Yang, W.T., Song, H.B., Wang, M., and Zhong, M.Y., 2009, Trace fossils and
815 ichnofabrics in the Heshanggou Formation of lacustrine deposits, Jiyuan Area,
816 Henan Province. Acta Sedimentologica Sinica, v. 27, p. 573–582 (in Chinese).
817 Ji, K.X., Wignall, P.B., Peakall, J., Tong, J.N., Chu, D.L., and Pruss, S.B., 2021,
818 Unusual intraclast conglomerates in a stormy, hot-house lake: the Early Triassic
819 North China Basin. Sedimentology, v.68, p. 3385–3404.
820 Ji, K.X., Wignall, P.B., Tong, J.N., Yu, Y.Y., Guo, W.W., Shu, W.C., and Chu, D.L.,
821 2022. Sedimentology of the latest Permian to Early Triassic in the terrestrial
822 settings of the North China Basin: Low-latitude climate change during a
823 warming-driven crisis. GSA Bulletin, https://doi.org/10.1130/B36260.1.
824 Jones, T.P., and Rowe, N.P., 1999, Fossil plants and spores: modern techniques.
825 Geological Society of London, pp. 420.
826 Kerp, H., 1990, The study of fossil gymnosperms by means of cuticular analysis.
827 Palaios, v. 5, 548–569.
828 Koll, R.A. and DiMichele, W.A., 2021. Dominance-diversity architecture of a mixed
829 hygromorphic-to-xeromorphic flora from a botanically rich locality in western
830 equatorial Pangea (lower Permian Emily Irish site, Texas, USA.
831 Palaeogeography, Palaeoclimatology, Palaeoecology, v. 563, art. 110132.
832 Kustatscher, E., Van Konijnenburg-Van Cittert, J.H.A., Bauer, K., Butzmann, R.,
833 Meller, B., and Fischer, T.C., 2012, A new flora from the Upper Permian of
834 Bletterbach (Dolomites, N–Italy). Review of Palaeobotany and Palynology, v.
835 182, p. 1–13.
836 Kustatscher, E., Bernardi, M., Petti, F.M., Franz, M., Van Konijnenburg-Van Cittert,
837 J.H.A., and Kerp, H., 2017, Sea-level changes in the Lopingian (late Permian) of

838 the northwestern Tethys and their effects on the terrestrial palaeoenvironments,
839 biota and fossil preservation. Global and Planetary Change, v. 148, p. 166–180.
840 Lee, M.S.Y., 1997, A taxonomic revision of pareiasaurian reptiles: implications for
841 Permian terrestrial palaeoecology. Modern Geology, v. 21, p. 231–298.
842 Liu, J., 2018, New progress on the correlation of Chinese terrestrial Permo-Triassic
843 strata. Vertebrata Palasiatica, v. 56, p. 327–342.
844 Liu, J., and Bever, G.S., 2018, The tetrapod fauna of the Upper Permian Naobaogou
845 Formation of China: A new species of *Elginia* (Parareptilia, Pareiasauria). Papers
846 in Palaeontology, v. 4, p. 197–209.
847 Liu, J., Xu, L., Jia, S.H., Pu, H.Y., and Liu, X.L., 2014, The Jiyuan tetrapod fauna of
848 the Upper Permian of China—2. stratigraphy, taxonomical review, and
849 correlation. Vertebrata Palasiatica, v. 52, p. 328–339.
850 Liu, J., and Sullivan, C., 2017, New discoveries from the *Sinokannemeyeria–*
851 *Shansisuchus* Assemblage Zone: 3. Archosauriformes from Linxian, Shanxi,
852 China. Vertebrata PalAsiatica, v. 55, p. 110–128.
853 Liu, J., Ramezani, J., Li, L., Shang, Q.H., Xu, G.H., Wang, Y.Y., and Yang, J.S.,
854 2018, High-precision temporal calibration of Middle Triassic vertebrate
855 biostratigraphy: U-Pb zircon constraints for the *Sinokannemeyeria* Fauna and
856 *Yonghesuchus*. Vertebrata PalAsiatica, v. 56, p. 16–24.
857 Liu, Y.Q., Kuang, H.W., Peng, N., Xu, H., Zhang, P., Wang, N.S., and An, W., 2015,
858 Mesozoic basins and associated palaeogeographic evolution in North China.
859 Journal of Palaeogeography, v. 4, p. 189–202.
860 Looy, C.V., Brugman, W.A., Dilcher, D.L., and Visscher, H., 1999, The delayed
861 resurgence of equatorial forests after the Permian–Triassic ecologic crisis.
862 Proceedings of the National Academy of Sciences, USA, v. 96, p. 13857–13862.

Looy, C.V., Twitchett, R.J., Dilcher, D.L., Van Konijnenburg-Van Cittert, J.H.A., and Visscher, H., 2001, Life in the end-Permian dead zone. Proceedings of the National Academy of Sciences, USA, v. 98, p. 7879–7883.

Lu, J., Zhang, P.X., Yang, M.F., Shao, Y.L., and Hilton, J., 2020, Continental records of organic carbon isotopic composition ($\delta^{13}C_{org}$), weathering, paleoclimate and wildfire linked to the End–Permian mass extinction, Chemical Geology, v. 558, p. 119764.

Mays, C., Vajda, V., Frank, T., Fielding, C., Nicoll, R.S., Tevyaw, A., and McLoughlin, S., 2020. Refined Permian-Triassic floristic timeline reveals early collapse and delayed recovery of south polar terrestrial ecosystems. GSA Bulletin, v. 132, p. 1489–1513.

Mays, C., McLoughlin, S., Frank, T.D., Fielding, C.R., Slater, S.M. and Vajda, V., 2021a. Lethal microbial blooms delayed freshwater ecosystem recovery following the end-Permian extinction. Nature communications, v. 12, p. 1–11.

Mays, C., Vajda, V. and McLoughlin, S., 2021b. Permian–Triassic non-marine algae of Gondwana—distributions, natural affinities and ecological implications. Earth-Science Reviews, v. 212, art. s103382.

McLoughlin, S., 2001, The breakup history of Gondwana and its impact on pre-Cenozoic floristic provincialism. Australian Journal of Botany, v. 49, p. 271–300.

McLoughlin, S., 2011, *Glossopteris*—insights into the architecture and relationships of an iconic Permian Gondwanan plant. Journal of the Botanical Society of Bengal, v. 65, p. 1–14.

McLoughlin, S., Nicoll, R.S., Crowley, J.L., Vajda, V., Mays, C., Fielding, C.R., Frank, T.D., Wheeler, A. and Bocking, M., 2021. Age and paleoenvironmental significance of the Frazer Beach Member—a new lithostratigraphic unit

888 overlying the end-Permian extinction horizon in the Sydney Basin, Australia.
889 Frontiers in Earth Science, v. 8, art. 600976.
890 Nesbitt, S.J., J. Liu and C. Li, 2011. A sail-backed suchian from the Heshanggou
891 Formation (Early Triassic: Olenekian) of China. Earth and Environmental
892 Science Transactions of the Royal Society of Edinburgh, v. 101, p. 271–284.
893 Niklas, K.J., Tiffney, B.H., and Knoll, A.H., 1983, Patterns in vascular land plant
894 diversification. Nature, v. 303, p. 614–616.
895 Nowak, H., Schneebeli-Hermann, E. and Kustatscher, E., 2019. No mass extinction
896 for land plants at the Permian–Triassic transition. Nature communications, v. 10,
897 p. 384.
898 Ouyang, S., and Norris, G., 1988, Spores and pollen from the Lower Triassic
899 Heshanggou Formation, Shaanxi Province, North China. Review of Palaeobotany
900 and Palynology, v. 54, p. 187–231.
901 Ouyang, S., and Wang, R.N., 1985, Age assignment of the Pingdingshan Member in
902 Henan and Anhui provinces. Experimental Petroleum Geology, v. 7, p. 141–147.
903 Ouyang, S., and Zhang, Z.L., 1982, Early Triassic palynological assemblage in
904 Dengfeng, Northwestern Henan. Acta Palaeontologica Sinica, v. 21, p. 685–696.
905 Pang, Q.Q.,1989, The Early–Middle Triassic stratigraphy and Ostracoda from the
906 Yima area in Henan province. Journal of Hebei College of Geology, v. 12, p.
907 325–345.
908 Qu, L.F., 1980, Triassic spore and pollen fossils. In: Institute of Geology, Chinese
909 Academy of Geological Sciences, Mesozoic stratigraphy and paleontology of the
910 Shaanxi-Gansu-Ningxia Basin. Vol. 1. Publishing House of Geology, Beijing,
911 China, p. 115–143.

912 Qu, L.F., 1982, The palynological assemblage from the Liujiagou Formation of
913 Jiaocheng, Shanxi. Bulletin of Geological Institute, Chinese Academy of
914 Geological Society, v. 4, p. 83–93.
915 Qu, L.F., Yang, J.D., Bai, Y.H., and Zhang, Z.L., 1983. A preliminary discussion on
916 the characteristics and stratigraphic divisions of Triassic spores and pollen in
917 China. Bulletin Chinese Academy of Geological Sciences, v. 5, p. 81–94.
918 Rees, P.M., 2002, Land-plant diversity and the end-Permian mass extinction. Geology,
919 v. 30, p.827–830.
920 Retallack, G.J., and Krull, E.S., 1999, Landscape ecological shift at the Permian-
921 Triassic boundary in Antarctica. Australian Journal of Earth Sciences, v. 46, p.
922 785–812.
923 Retallack, G.J., Veevers, J.J., and Morante, R., 1996, Global coal gap between
924 Permian-Triassic extinction and Middle Triassic recovery of peat–forming plants.
925 Geological Society of America Bulletin, v. 108, p. 195–207.
926 Scotese, C.R., 2021. An Atlas of Phanerozoic Paleogeographic Maps: The seas come
927 in and the seas go out. Annual Review of Earth and Planetary Sciences, v. 49, p
928 679–728.
929 Sephton, M.A., Jiao, D., Engel, M.H., Looy, C.V., and Visscher, H., 2015, Terrestrial
930 acidification during the end-Permian biosphere crisis? Geology, v. 43, p. 159–
931 162.
932 Sepkoski J. J. Jr., 1984, Kinetic model of Phanerozoic taxonomic diversity. III. Post–
933 Paleozoic families and mass extinctions. Paleobiology, v. 10, p. 246–267.
934 Shen, W.J., Sun, Y.G., Lin, Y.T., Liu, D.H., and Chai, P.X., 2011, Evidence for
935 wildfire in the Meishan section and implications for Permian–Triassic events.
936 Geochimica et Cosmochimica Acta, v. 75, p. 1992–2006.

937 Shu, W.C., Tong, J.N., Tian, L., Benton, M.J., Chu, D.L., Yu, J.X., and Guo, W.W.,
938 2018, Limuloid trackways from Permian-Triassic continental successions of
939 North China. Palaeogeography, Palaeoclimatology, Palaeoecology, v. 508, p. 71–
940 90.
941 Song, H.J., Wignall, P.B., Tong, J.N., Song, H.Y., Chen, J., Chu, D.L., Tian, L., Luo,
942 M., Zong, K.Q., Chen, Y.L., Lai, X.L., Zhang, K.X., and Wang, H.M., 2015,
943 Integrated Sr isotope variations and global environmental changes through the
944 Late Permian to early Late Triassic. Earth and Planetary Science Letters, v. 424,
945 p. 140–147.
946 Stanley, S.M., 2016. Estimates of the magnitudes of major marine mass extinctions in
947 earth history. Proceedings of the National Academy of Sciences, v. 113, p.
948 E6325–E6334.
949 Stevens, L.G., Hilton, J., Bond, D.P.G., Glasspool, I.J., and Jardine, P.E., 2011,
950 Radiation and extinction patterns in Permian floras from North China as
951 indicators for environmental and climate change. Journal of the Geological
952 Society, London, v. 168, p. 607–619.
953 Sun, Y.D., Joachimski, M.M., Wignall, P.B., Yan, C.B., Chen, Y.L., Jiang, H.S.,
954 Wang, L.N., and Lai, X.L., 2012, Lethally hot temperatures during the Early
955 Triassic Greenhouse. Science, v. 338, p. 366–370.
956 Tong, J.N., Chu, D.L., Liang, L., Shu, W.C., Song, H.J., Song, T., Song, H.Y., and
957 Wu, Y.Y., 2018, Triassic integrative stratigraphy and timescale of China. Science
958 China Earth Sciences, v. 62, p. 189–222.
959 Tu, C.Y., Chen, Z.Q., Retallack, G.J., Huang, Y.G., and Fang,Y.H., 2016,
960 Proliferation of MISS–related microbial mats following the end-Permian mass
961 extinction in terrestrial ecosystems: Evidence from the Lower Triassic of the

962 Yiyang area, Henan Province, North China. Sedimentary Geology, v. 333, p. 50–
963 69.
964 Vajda, V., McLoughlin, S., Mays, C., Frank, T.D., Fielding, C.R., Tevyaw, A.,
965 Lehsten, V., Bocking, M., and Nicoll, R.S., 2020, End-Permian (252 Mya)
966 deforestation, wildfires and flooding—An ancient biotic crisis with lessons for
967 the present. Earth and Planetary Science Letters, v. 529, p. 115875.
968 Visscher, H., Looy, C.V., Collinson, M.E., Brinkhuis, H., van Konijnenburg-van
969 Cittert, J.H.A., Kürschner, W.M., and Sephton, M.A., 2004, Environmental
970 mutagenesis during the end-Permian ecological crisis. Proceedings of the
971 National Academy of Sciences, USA, v. 101, p. 12952–12956.
972 Wang, J., 2010. Late Paleozoic macrofloral assemblages from Weibei Coalfield, with
973 reference to vegetational change through the Late Paleozoic Ice-age in the North
974 China Block. International Journal of Coal Geology, v. 83, p. 292–317.
975 Wang, J., Liu, H.Q., Shen, G.L., and Zhang, H., 1998, Notes on the island distribution
976 pattern of the Permian Cathaysian flora in China: an example of the application
977 of the equilibrium theory of island biogeography in palaeobiogeography.
978 Palaeogeography Palaeoclimatology Palaeoecology, v. 142, p. 23–31.
979 Wang, J.Y., Yi, J., Liu, J., 2019, The first complete pareiasaur skull from China. Acta
980 Palaeontologica Sinica, v. 58, p. 216–221.
981 Wang, L.X., 1983. Triassic of Shanxi. Shanxi Provincial Geological Prospecting
982 Bureau, 198 pp.
983 Wang, L.X., Xie, Z.M., and Wang, Z.Q., 1978, On the occurrence of *Pleuromeia* from
984 the Qinshui basin in Shanxi province. Acta Palaeontologica Sinica, v. 17, p. 195–
985 211.

986 Wang R.N., 1981, The “Shichienfeng Formation” of Yongcheng, Henan province and
987 other adjacent area. Journal of Stratigraphy, v. 5, p. 180–189.
988 Wang, Z.Q., 1993, Evolutionary ecosystem of Permian–Triassic redbeds in North
989 China: a historical record of global desertification. New Mexico Museum of
990 Natural History and Science Bulletin, v. 3, p. 471–476.
991 Wang, Z.Q., 1996, Recovery of vegetation from the terminal Permian mass extinction
992 in North China. Review of Palaeobotany and Palynology, v. 91, p. 121–142.
993 Wang, Z.Q., and Wang, L.X., 1982, A new species of the lycopsid *Pleuromeia* from
994 the early Triassic of Shanxi, China and its ecology. Palaeontology, v. 25, p. 215–
995 225.
996 Wang, Z.Q., and Wang, L.X., 1986, Late Permian fossil plants from the lower part of
997 the Shiqianfeng (Shihchienfeng) group in North China. Bulletin Tianjin Institute
998 of Geology and Mineral Resources, v. 15, p. 1–120.
999 Wignall, P.B., 2015, The worst of times. Princeton University Press, p. 64–75.
1000 Wu, Q., Ramezani, J., Zhang, H., Wang, J., Zeng, F.G., Zhang, Y.C., Liu, F., Chen, J.,
1001 Cai, Y.F., Hou, Z.S., Liu, C., Yang, W., Henderson, C.M. and Shen, S.Z., 2021,
1002 High-precision U-Pb age constraints on the Permian floral turnovers,
1003 paleoclimate change, and tectonics of the North China block. Geology, v. 49, p.
1004 677–681.
1005 Wu, Y.Y., Tong, J.N., Algeo, T.J., Chu, D.L., Cui, Y., Song, H.Y., Shu, W.C., and Du,
1006 Y., 2020, Organic carbon isotopes in terrestrial Permian-Triassic boundary
1007 sections of North China: Implications for global carbon cycle perturbations.
1008 Geological Society of America Bulletin, v. 132, p. 1106–1118.

1009 Xiong, C.H., and Wang, Q., 2011, Permian–Triassic land-plant diversity in South
1010 China: Was there a mass extinction at the Permian/Triassic boundary?
1011 Paleobiology, v. 37, p. 157–167.
1012 Xu, L., Li, X.W., Jia, S.H. and Liu, J., 2015, The Jiyuan tetrapod Fauna of the Upper
1013 Permian of China: New pareiasaur material and the reestablishment of *Honania*
1014 *complicidentata*. Acta Palaeontologica Polonica, v. 60, p.689–700.
1015 Xu, Z., Hilton, J., Yu. J.X., Wignall, P.B., Yin, H.F., Xue, Q., Ran, W.J., Hui, L.,
1016 Shen, J., and Meng, F.S., 2022. Mid-Permian to Late Triassic plant species
1017 richness and abundance patterns in South China: Co-evolution of plants and the
1018 environment through the Permian-Triassic transition. Earth-Science Reviews.
1019 https://doi.org/10.1016/j.earscirev.2022.104136
1020 Yang, G.X., and Wang, H.S., 2012, Yuzhou Flora- A hidden gem of the Middle and
1021 Late Cathaysian Flora. Science China Earth Sciences, v. 55, p. 1601–1619.
1022 Yin, H.F., and Lin, H.M., 1979, Marine Triassic faunas and the geologic time from
1023 Shihchienfeng Group in the northern Weihe River Basin, Shaanxi Province. Acta
1024 Stratigraphica Sinica, v. 3, p. 233–241 (in Chinese).
1025 Yu, J.X., Broutin, J., Chen, Z.Q., Shi, X., Li, H., Chu, D.L., and Huang, Q.S., 2015,
1026 Vegetation changeover across the Permian–Triassic Boundary in Southwest
1027 China: extinction, survival, recovery and palaeoclimate: A critical review. Earth-
1028 Science Reviews, v. 149, p. 203–224.
1029 Yu, Y.Y., Tian, L., Chu, D.L., Song, H.Y., Guo, W.W. and Tong, J.N., 2022, Latest
1030 Permian–Early Triassic paleoclimatic reconstruction by sedimentary and isotopic
1031 analyses of paleosols from the Shichuanhe section in central North China Basin.
1032 Palaeogeography, Palaeoclimatology, Palaeoecology, v. 585, p.110726.

1033 Zheng, D., Chang, S.C., Wang, H., Fang, Y., Wang, J., Feng, C., Xie, G.,
1034 Jarzembowski, E.A., Zhang, H., and Wang, B., 2018, Middle-Late Triassic insect
1035 radiation revealed by diverse fossils and isotopic ages from China. Science
1036 advances, v. 4, p. eaat1380.
1037 Zhu, R.K., Xu, H.X., Deng, S.H., and Guo, H.L., 2007, Lithofacies palaeogeography
1038 of the Permian in northern China. Journal of Palaeogeography, v. 9, p. 133–142.
1039 Zhu, Z.C., Kuang, H., Liu, Y.Q., Benton, M.J., Newell, A.J., Xu, H., An, W., Ji, S.A.,
1040 Xu, S.C., Peng, N., and Zhai, Q.G., 2020, Intensifying aeolian activity following
1041 the end-Permian mass extinction: evidence from the Late Permian–Early Triassic
1042 terrestrial sedimentary record of the Ordos Basin, North China. Sedimentology, v.
1043 67, p. 2691–2720.

1044

1045 **FIGURES AND TABLES CAPTIONS**

1046 Figure 1. (A) Late Permian paleophytogeographical maps and distribution of typical
1047 Early Triassic fossil plant taxa during the Late Permian to Early Triassic (Broutin et al.
1048 1995; McLoughlin 2001, 2011); base map adapted from Scotese (2021). (B)
1049 Paleogeographic map of the Late Permian and main sections of this study in North
1050 China; base map modified from Zhu et al. (2007). (C) Palaeogeographic map of the
1051 Early Triassic and main sections of this study in North China; base map modified
1052 from Liu et al. (2015). (D) Geographic distributions of fossil plant locations from the
1053 Sunjiagou (SJG), Liujiagou (LJG), Heshanggou (HSG) and Ermaying (EMY)
1054 formations in North China (Supplementary Data File 1).

1055

1056 Figure 2. Lithological columns of the studied sections showing the lithology and the
1057 position of the fossil horizons and some special sedimentary structures. Lower dotted

line marks the end-Permian Plant Extinction event (EPPE), the gray area indicates the ecological disturbance interval without fossil plants, and the upper dashed line marks the occurrence of Early Triassic fossil plants in the studied sections. Abbreviation: Fm., Formation, Tetra., Tetrapods.

Figure 3. Plant fossils, cuticles and *in situ* pollens from the top part of the Upper Shihhotse Formation of the Shichuanhe and Liulin sections. A–C, *Autunia*–type ovuliferous organs. D, small fragmentary pinna of *Sphenopteris*. E, F, strap-like leaf in E and broken leaf in F of *Taeniopteris* with simple parallel lateral veins arising from the midvein at an angle of nearly 90°. G–J, broken leaves of ginkgophytes, G and H, broken leaves of ginkgophyte type 2 with horn-like shape and dichotomous-patterned veins, I and J, broken wedged-shape leaves with the bifurcated rounded apex of ginkgophyte type 1 with strong petioles. K–O, T, W, shoots and cuticle of conifer type 2, K with possible terminate cone on the shoot, the cuticle in W is from the shoot in T. P, possible cone of a conifer. Q–S, U, V, X, Y, shoots, cuticles and *in situ* pollens of conifer type 0, U and V are cuticles macerated from the shoot in S, X and Y are *in situ* pollens "picked out" directly from the shoots in Q–S and pollen in Y was photographed under SEM. Scale bars: A–D, L, T are 5 mm. E–K, M–S are 1 cm. U, V, X, Y are 50 μm, W is 20 μm. A–D, F, I–J, K–O, P from the Shichuanhe section. E, G–H, Q–T, Q–Y from the Liulin section.

Figure 4. Plant fossils, cuticles and *in situ* pollens from the lower part of the Sunjiagou Formation of the Liulin, Dayulin and Zishiya sections. A, fragments of pinnule of pteridophyte with dichotomous veins. B–I, M–O, vegetative terminal pinnae of *Germaropteris martinsii* and its cuticles, triangular arrows in N and O show

the base of trichome, D before processing, E after processing, F–I and M–O are from the red rectangular area of E. J–L, fertile parts of the *Autunia*-type organ. P–Y, MM, shoots and isolated leaves of conifer type 3 of *Pseudovoltzia* with well-preserved cuticle, R–X are from Q, S–X is from the red rectangular area of R. AA, bract-scale complexes of fossil conifers. BB–CC, heterophyll shoot and its cuticles of conifer type 2. DD, EE, PP, SS, male cone of conifer and its *in situ* pollens (possible *Gardenasporites*), EE is a reconstruction of DD, PP is the distal view and SS is the proximal view of pollen grains. FF–GG, some shoots of conifer type 4. Z, HH–LL, NN, OO, QQ, RR, some conifer shoots with their cuticles of conifer type 1. Scale bars: A, J, Y, Z, AA, BB are 5 mm. K, L, DD–HH, KK, LL, MM are 1 cm. B–E, P–R are 1 mm. F–I, N–O, T–X, CC, NN–SS are 50 μm; M, S, II are 500 μm; JJ is 200 μm. A–J, M–O, DD–GG, PP, SS from the Liulin section. P–Z, AA–CC, HH–JJ, NN–OO, QQ, RR from the Dayulin section. K, L, KK–MM from the Zishiya section.

Figure 5. Strobili of *Pleuromeia* and pinnate fragments of pteridophylls from the upper part of the Liujiagou Formation at Peijiashan. A, B, pinnate fragments of *Scolopendrites*. C–K, strobili of *Pleuromeia*. F–K was processed under CT scanning. All scale bars are 1 cm.

Figure 6. *In situ* stems/rhizomorphs and dispersed megasporophylls of *Pleuromeia*, dispersed broken megasporophylls of *Tomiostrobus*, *in situ* rhizomes and dispersed stems of *Neocalamites* and *Equisetites* and isolated possible male cone, bract-scale complexes and seeds of voltzian conifers from the basal Heshanggou Formation of Heshun. A–D, *in situ* stems/rhizomorphs of *Pleuromeia*, C is the bottom of B showing four-lobed rhizomorphs. E–J, some *in situ* rhizomes and dispersed stems of

Neocalamites, F, triangular arrow shows the linear whorled leaves at the node; H, triangular arrow shows one small branch base at the node; J, shows the underground part of the rhizome and triangular arrow shows the upright stem. K shows broken stem of *Equisetites*. L, dispersed broken megasporophyll with a long tip characteristic of *Tomiostrobus*. M, dispersed megasporophyll of *Pleuromeia*. N, one isolated possible male cone. O, bract-scale complexes and cordiform seeds of voltzian conifers. Scale bars: A, B, D, J are 5 cm; C is 2 cm; E–I, K–O are 1 cm.

Figure 7. Plants from the Lower Heshanggou Formation of Yushe. A–D, megasporophylls of *Pleuromeia*, some microconchids on the surface of D at the triangular arrow. E, F, pinnae of *Anomopteris*. G, stem of *Pleuromeia*. H, strobilus of *Pleuromeia*. I, the broken stem of *Neocalamites*. J–L, *in situ* rhizophores of *Pleuromeia*. M–O, leaves of *Tongchuanophyllum*, showing feeding holes on the surface and margins of O at the triangular arrow. P–Q, bract-scale complexes of voltzian conifers. Scale bars: A, C, F, Q are 5 mm; B, D, E, G–P are 1 cm.

Figure 8. Some plant fossils from the Ermaying Formation of Yushe. A–C, some rhizophores of *Pleuromeia*. D–F, some broken sphenophyte stems of probably *Neocalamites*, showing possible invertebrate burrows inside the cast of the stem F. G–I, some woody plant fossil wood casts. Scale bars: A–D are 1 cm; E–I are 5 cm.

Figure 9. Other fossils associated with fossil plants. A–D, CT scanned 3D photos of Temnospondyli tooth from fossil-plant-bearing horizon of the Upper Shihhotse Formation in the Shichuanhe section showing well-preserved inner structure; E, fragment of insect wing fossil; F, many microconchids found on some plant remains;

G, some ophiurids; H–K, M, R, some conchostracans (H–K, *Pseudestheria* spp.; M, *Euestheria gutta*; R, *Magniestheria mangaliensis*); L, some lingulids; N–Q, S, T, some bivalves (N, *Pteria ussurica variabilis*; O, *Wilkingia* sp.; P, *Modiolus* sp.; Q, *Leptochondria* sp.; S, *Palaeoneilo elliptica*; T, *Promyalina putiatinensis*). Scale bars: A–G, O, P, T is 1 cm; H–N, Q–S is 1 mm. E, F, L–N were found in the rich sporomorph horizon of the Sunjiagou Formation in the Shichuanhe section; G and R were found in rich sporomorph horizon of the Qishan Formation in the Zishiya section; H-K were found with fossil plants in the Lower Sunjiagou Formation, H–J, in the Liulin section; K, in the Dayulin section; O–Q, S, T were found in the fossil-plant-bearing horizon of the Sunjiagou Formation in the Zishiya section.

Figure 10. Range chart of floras from North China from the Cisuralian to Middle Triassic interval. Five floras, one of which includes two sub-floras, and five floral transitions including an extirpation event, two turnovers and two radiation events are recognized here (Supplementary Data File 2, 3). g. extinction, gigantopterid flora extirpation; T1–T5, floral transition 1–5; EPPE, end-Permian Plant Extinction event. References of the previous studies can be seen in Supplementary Data File 4. Plant zones or subzones or assemblages in previous studies (see Supplementary Data File 4): *CrS*Z, *PZ*, *UZ*, *PjS*Z, *PeS*Z, *PsS*Z, *TZ*, *IS*Z, *SS*Z, *GLF*, *GLP*, *UY*, *GMLF*, *MPL*, *PSP*, *UP*; floras in this study (see Supplementary Data File 4): Voltziales, the Voltziales flora; gw, the ginkgophyte–walchian Voltziales subflora; Voltz., the voltzian Voltziales subflora; *PN*, the *Pleuromeia–Neocalamites* flora; *PT* flora, the *Pleuromeia–Tongchuanophyllum* flora; *LV* flora, the *Lepacyclotes–Voltzia* flora. Te., tectonism; Wu., Wuchiapingian.

Figure 11. Hierarchical clustering and *k*–means clustering for five floras and three main phases from Permian to Middle Triassic in North China. A. Hierarchical clustering–complete linkage analysis showing five different floras from Permian to Middle Triassic in North China; B. k–means clustering analysis showing three main phases from Lopingian to Middle Triassic in North China. a. the gigantopterid flora extirpation (T1) and the absence of the coal deposits, b. End-Permian Plant extinction (EPPE, T3), c. Gradual recovery of floras (T5). gigantopter. flora, the gigantopterid flora; Volt. flora, the Voltziales flora; *PN* flora, the *Pleuromeia–Neocalamites* flora; *PT* flora, the *Pleuromeia–Tongchuanophyllum* flora; *LV* flora, the *Lepacyclotes–Voltzia* flora. 1–5, cluster centroids; T1–T5, floral transition 1–5.

Figure 12. Model of floral community's changeovers associated with different animals during the Permian–Triassic crisis in North China. 1, *Tomiostrobus*/*Lepacyclotes*; 2. *Pleuromeia*; 3. *Sphenophytes*; 4, 19. Tree ferns; 5. Small Pteridophytes (e.g., *Anomopteris*/*Scolopendrites*); 6. Pteridosperms; 7. Cycads; 8. Ginkgophytes; 9. Conifers; 10. Ostracods; 11. Conchostracans; 12. Triopsidae; 13. Bivalves; 14. Insects; 15. Fishes; 16. MISS; 17. Lingulids; 18. *Yuania*; 20. gigantopterids; 21. Lepidodendrales. TED interval, the terrestrial ecological disturbance interval; LMUUSHZ, Lower–Middle–Upper Upper Shihhotse Formation; tUSHZ, topmost Upper Shihhotse Formation; Fm., Formation; g. extinction, gigantopterid flora extinction; T1–T5, floral transition 1–5; EPPE, end-Permian plant extinction event.

Figure 13. Late Permian to Triassic biotic and environmental changes in North China. Including diversity of plant, insect, tetrapod, fish, invertebrate and trace fossils

associated with the environmental changes of coal deposits, red beds and humid/arid climates. Changes of coal deposits and red beds are modified from Wang (2010) and other data in Supplementary Data File 2–9. Fms, Formations; USHZ, the Upper Shihhotse Formation; SJG, the Sunjiagou Formation; LJG, the Liujiagou Formation; HSG, the Heshanggou Formation; EMY, the Ermaying Formation; Spo., Sporomorph assemblages; Cisura., Cisuralian; Loping., Lopingian; Wu.–Cha., Wuchiapingian–Changhsingian. TED interval is terrestrial ecological disturbance interval; gig. flora, the gigantopterid flora; Volt. flora, the Voltziales flora; *PN* flora, the *Pleuromeia–Neocalamites* flora; *PT* flora, the *Pleuromeia–Tongchuanophyllum* flora; *LV* flora, the *Lepacyclotes–Voltzia* flora. Sporomorph assemblages: *Patellisporites meishanensis* biozone (*Pm*); *Lueckisporites virkkiae–Jugasporites schaubergeroides* assemblage (*LvJs*); *Aratrisporites–Alisporites* assemblage (*AA*); *Densoisporites nejburgii–Lunatisporites–Cycadopites* assemblage (*DnLC*); *Cycadopites–Lunatisporites–Verrucosisporites* assemblage (*CLV*); *Punctatisporites–Chordasporites* (*PC*) assemblage see in Fig. S2; bioturbation intensity (The Bedding Plane Bioturbation Index (BPBI) and ichnofabric index (ii)) data from (Guo et al., 2019). Dashed lines mark position of two losses of diversity, the lowermost an extirpation event and the upper extinctions of the EPPC; three dotted lines mark position of three transitions the lowermost a turnover, the upper two radiations; gE, gigantopterid flora extirpation; T1–T5, floral transition 1–5; EPPE, end-Permian Plant Extinction event.

TABLE 1. THE NUMBER OF SPECIMENS OF MACROFOSSIL PLANTS FROM DIFFERENT FORMATIONS AND SECTIONS OF NORTH CHINA IN THIS STUDY.

Liulin Section	Peijiashan Section	Dayulin Sectio	Shichuanhe Section	Zishiya Section	Heshun Section	Yushe Section	Pingyao Section	T.

			n						
HSG Fm.							280	120	400
LJG Fm.		80		10		10			100
SJG Fm.	206		37		202				445
USH Fm.	46			385					432
T.	252	80	37	395	202	10	280	120	133 7

Notes: USH Fm., Upper Shihhotse Formation; SJG Fm., Sunjiagou Formation; LJG Fm., Liujiagou Formation; HSG Fm., Heshanggou Formation; T., total specimens.

1207

1208

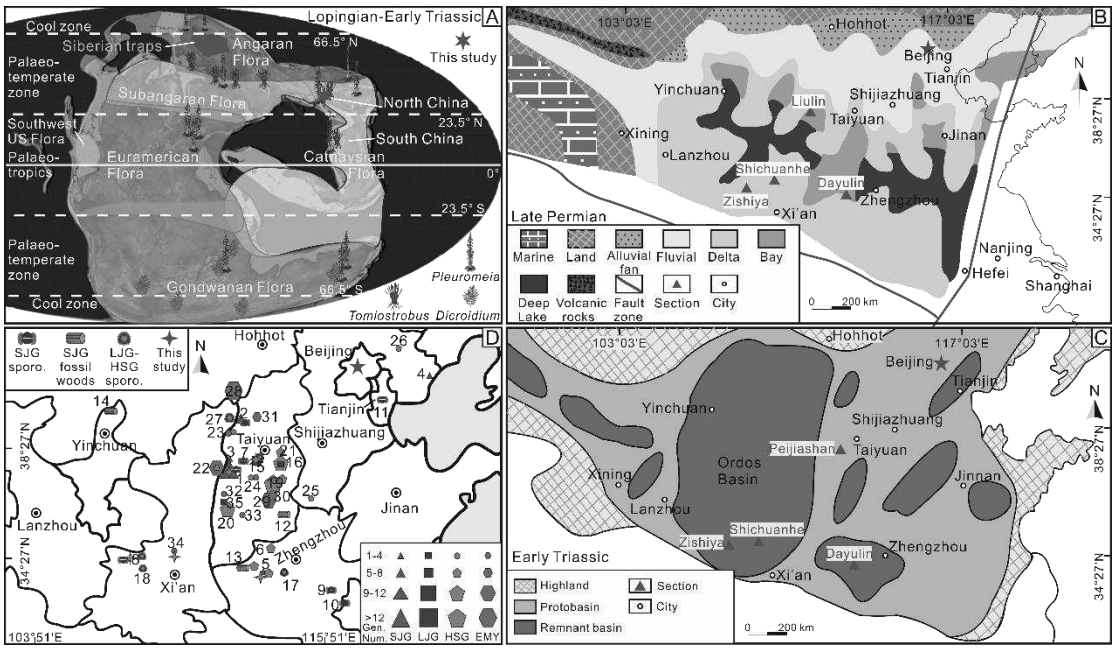

1209

1210 Figure 1

1211

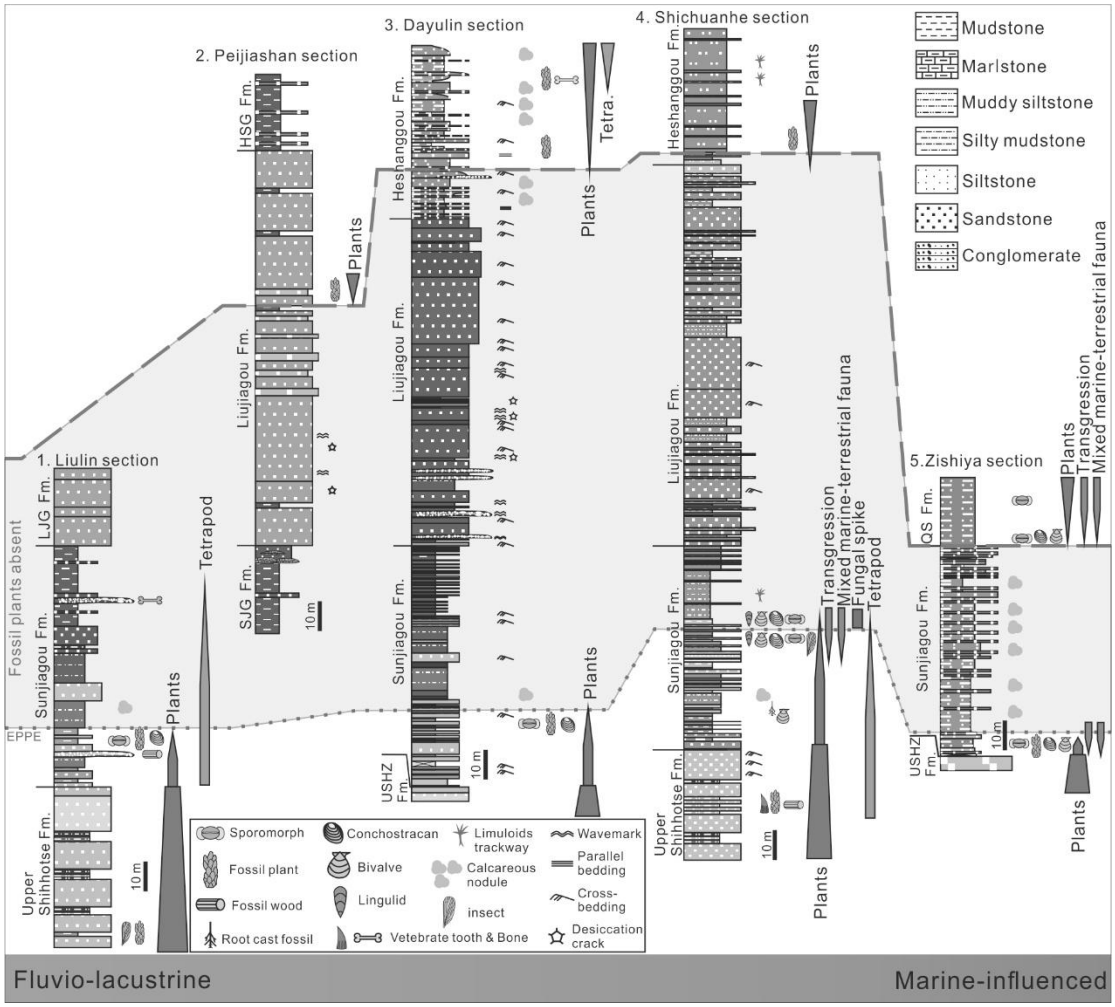
1. Liulin section
2. Peijiashan section
3. Dayulin section
4. Shichuanhe section
5.Zishiya section
Mudstone
Marlstone
Muddy siltstone
Silty mudstone
Siltstone
Sandstone
Conglomerate
Fossil plants absent
LJG Fm.
Sunjiagou Fm.
HSG Fm.
SJG Fm.
Liujiagou Fm.
Heshanggou Fm.
USHZ Fm.
QS Fm.
Upper Shihhotse Fm.
EPPE
Tetrapod
Plants
Tetra.
Transgression
Mixed marine-terrestrial fauna
Fungal spike
Mixed marine-terrestrial fauna
10 m
Sporomorph
Fossil plant
Fossil wood
Root cast fossil
Conchostracan
Bivalve
Lingulid
Vetebrate tooth & Bone
Limuloids trackway
Calcareous nodule
insect
Wavemark
Parallel bedding
Cross-bedding
Desiccation crack
Fluvio-lacustrine
Marine-influenced

Figure 2

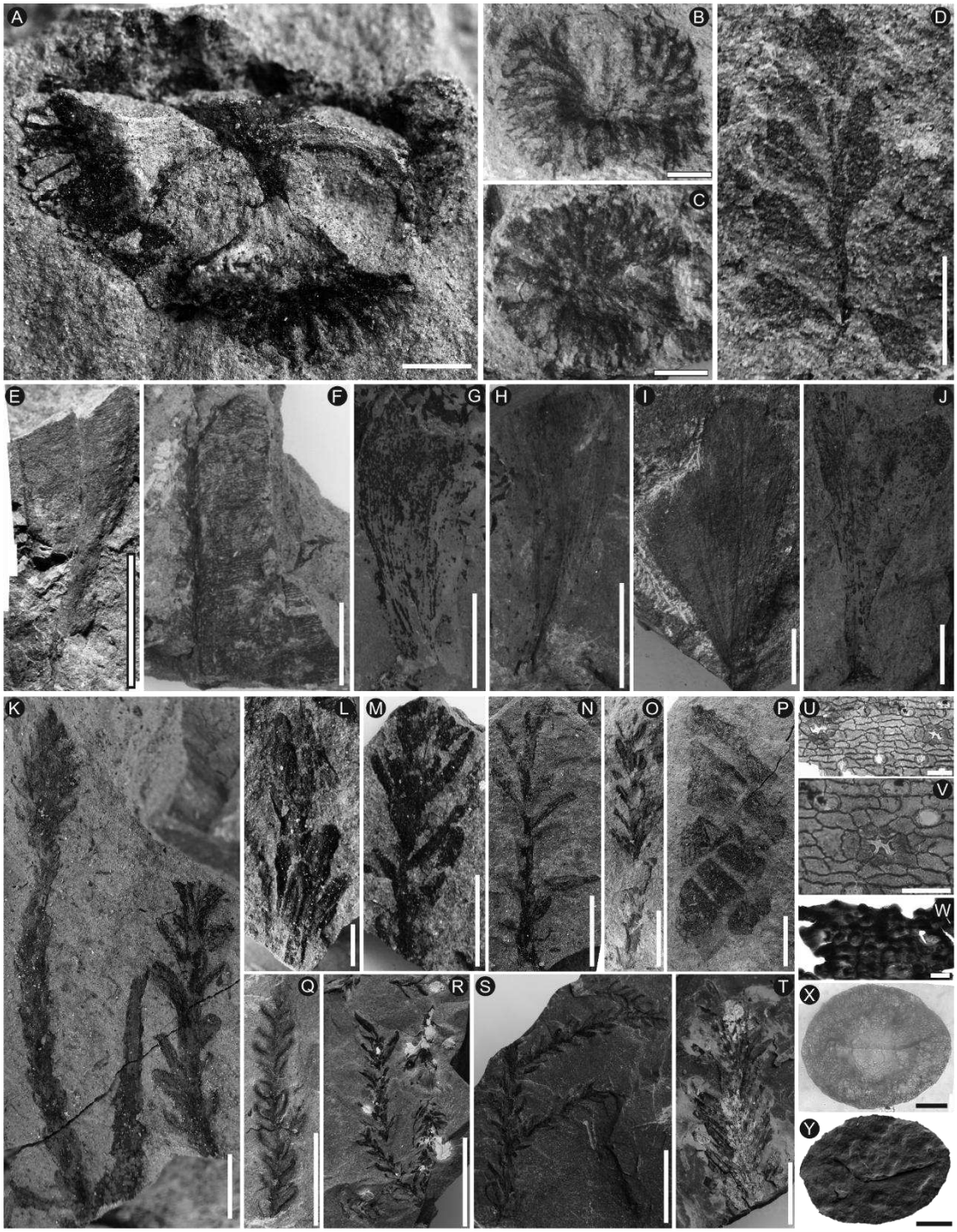

1215

1216 Figure 3

1217

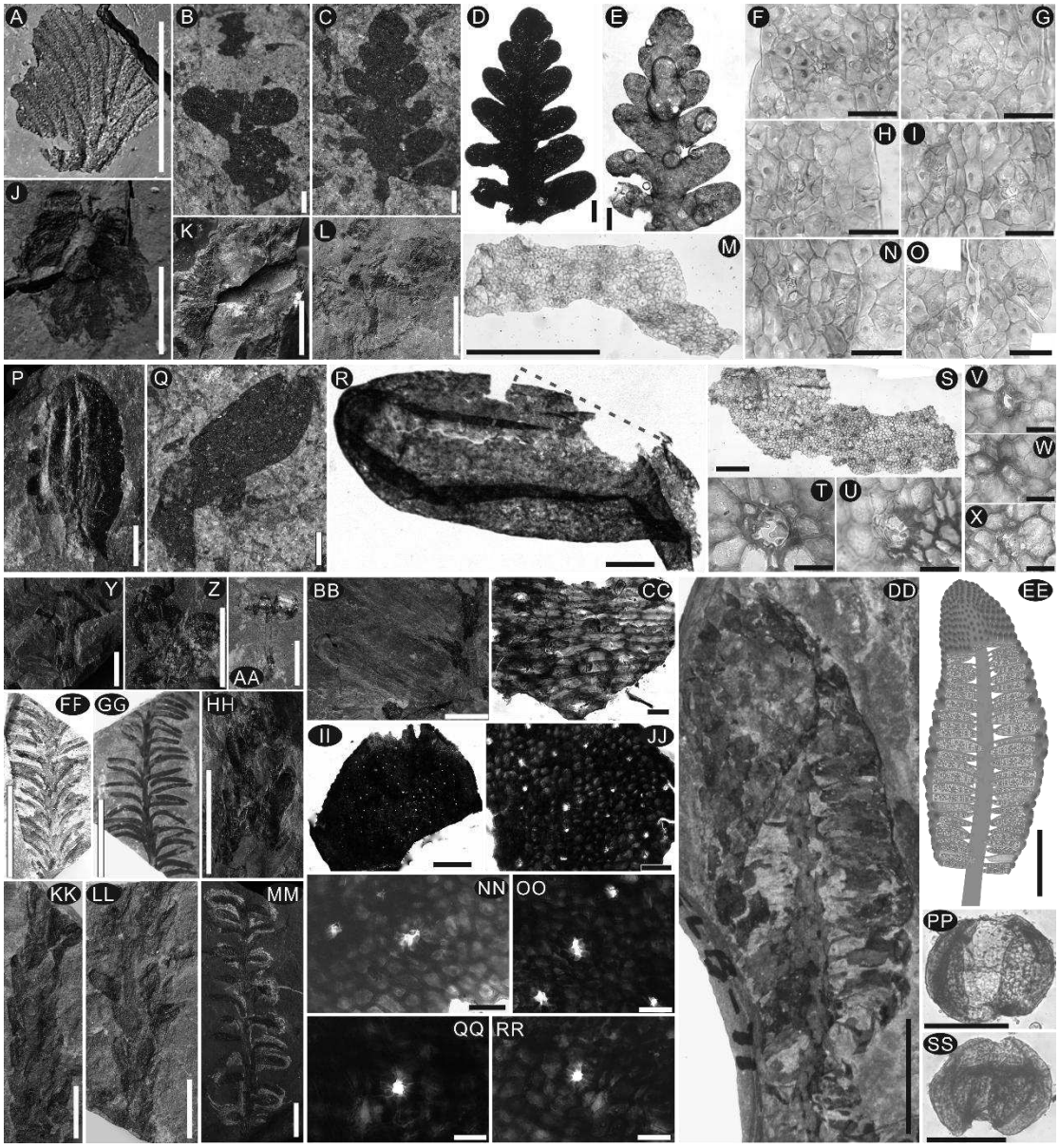

1218

1219 Figure 4

1220

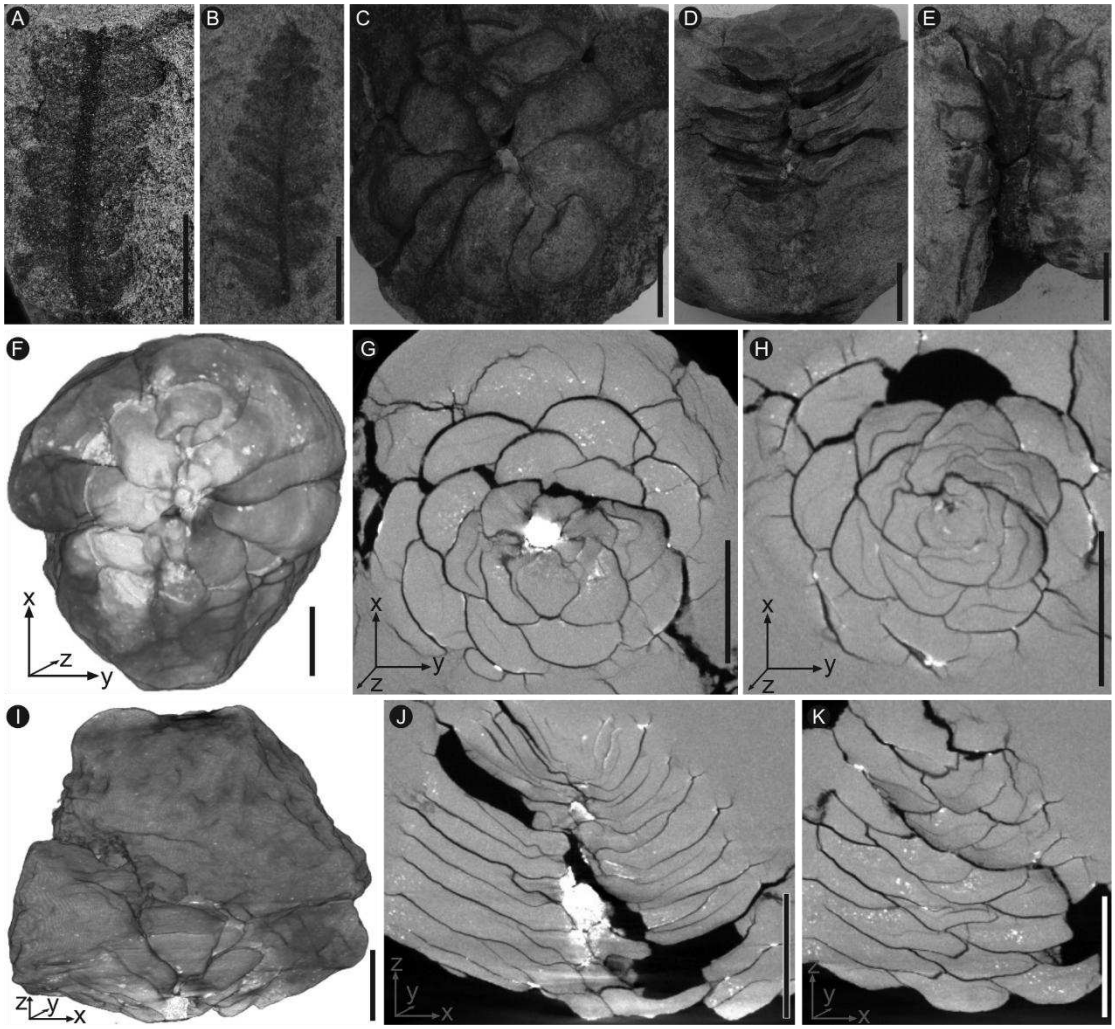

Figure 5

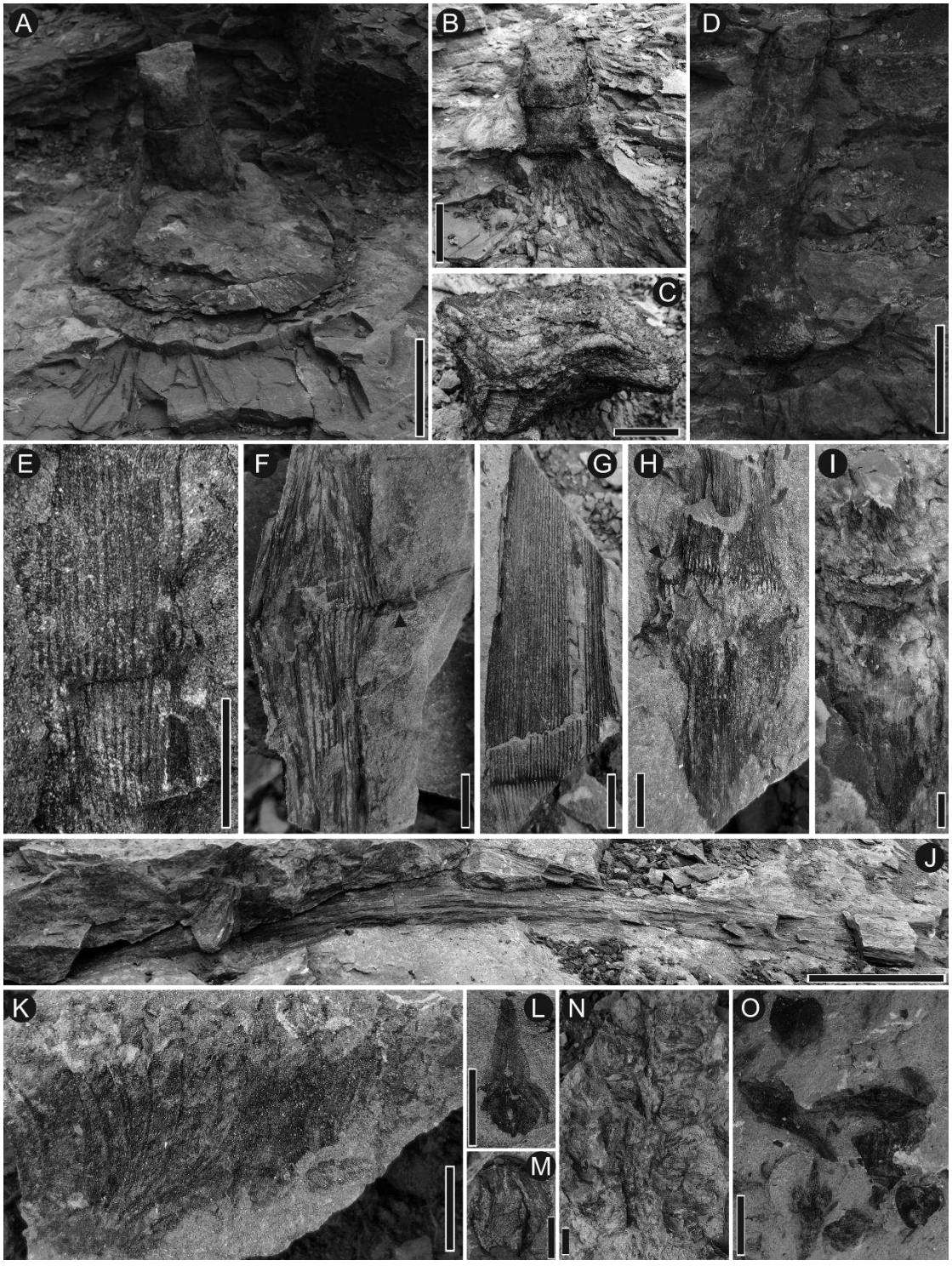

1224

1225 Figure 6

1226

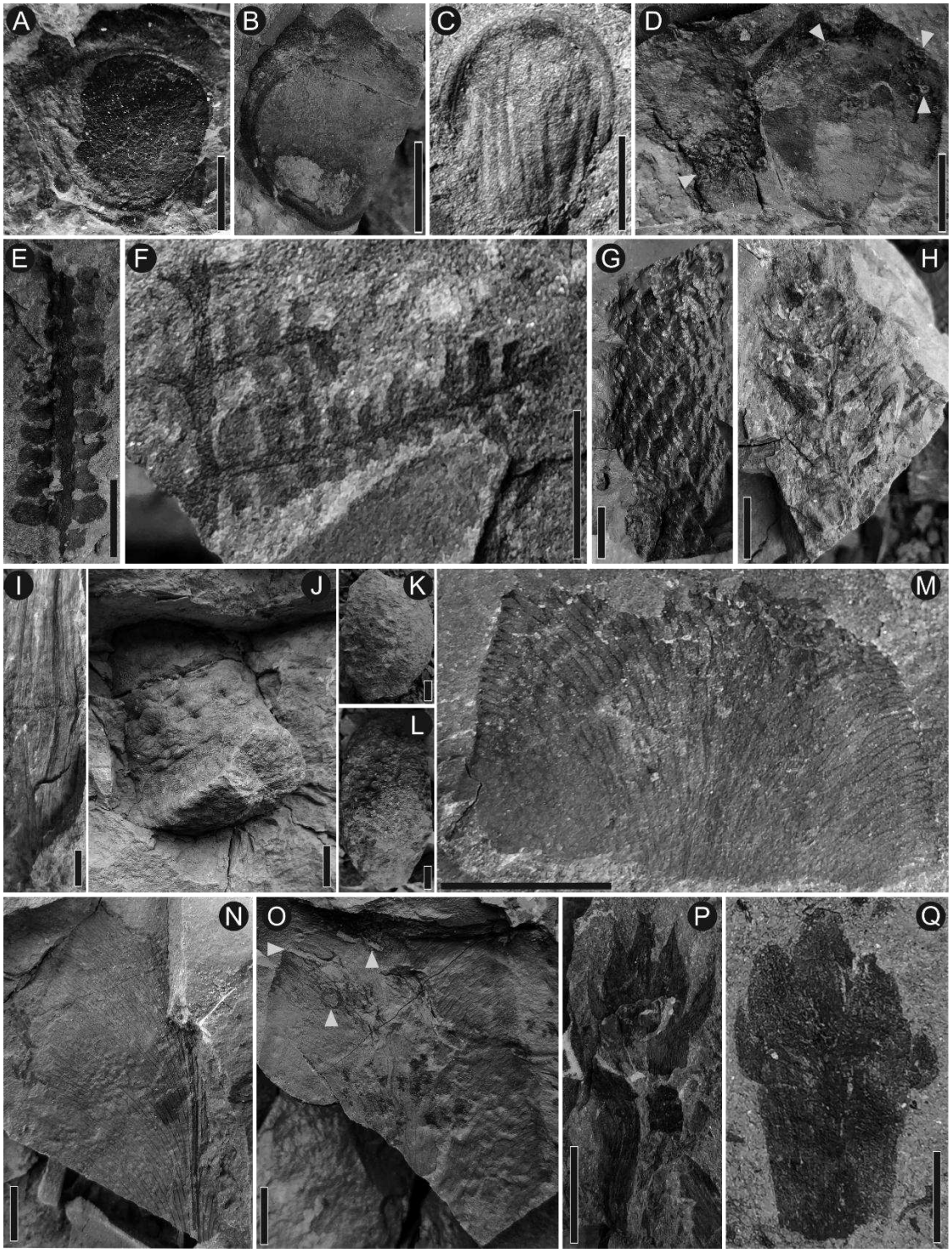

1227

1228 Figure 7

1229

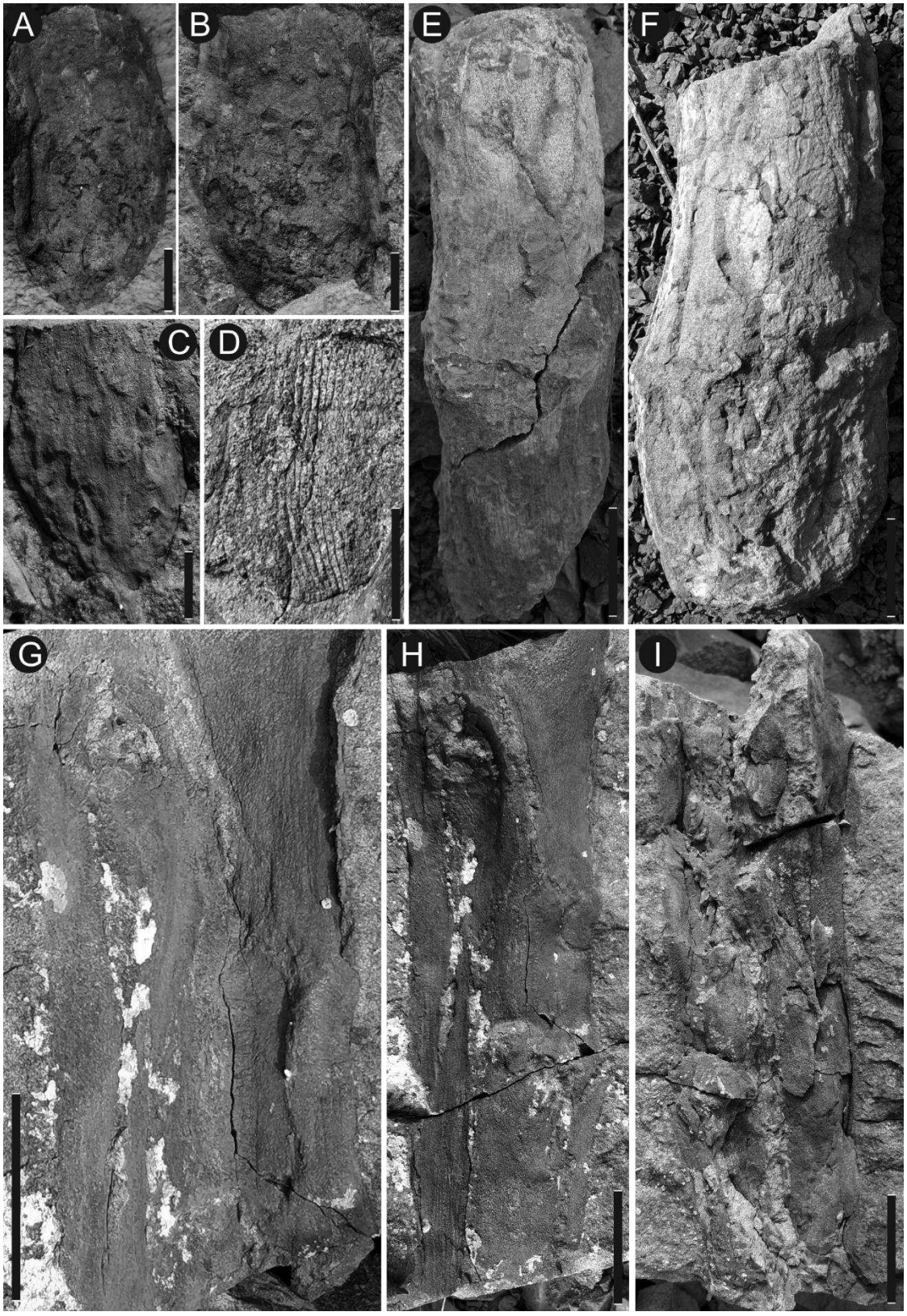

Figure 8

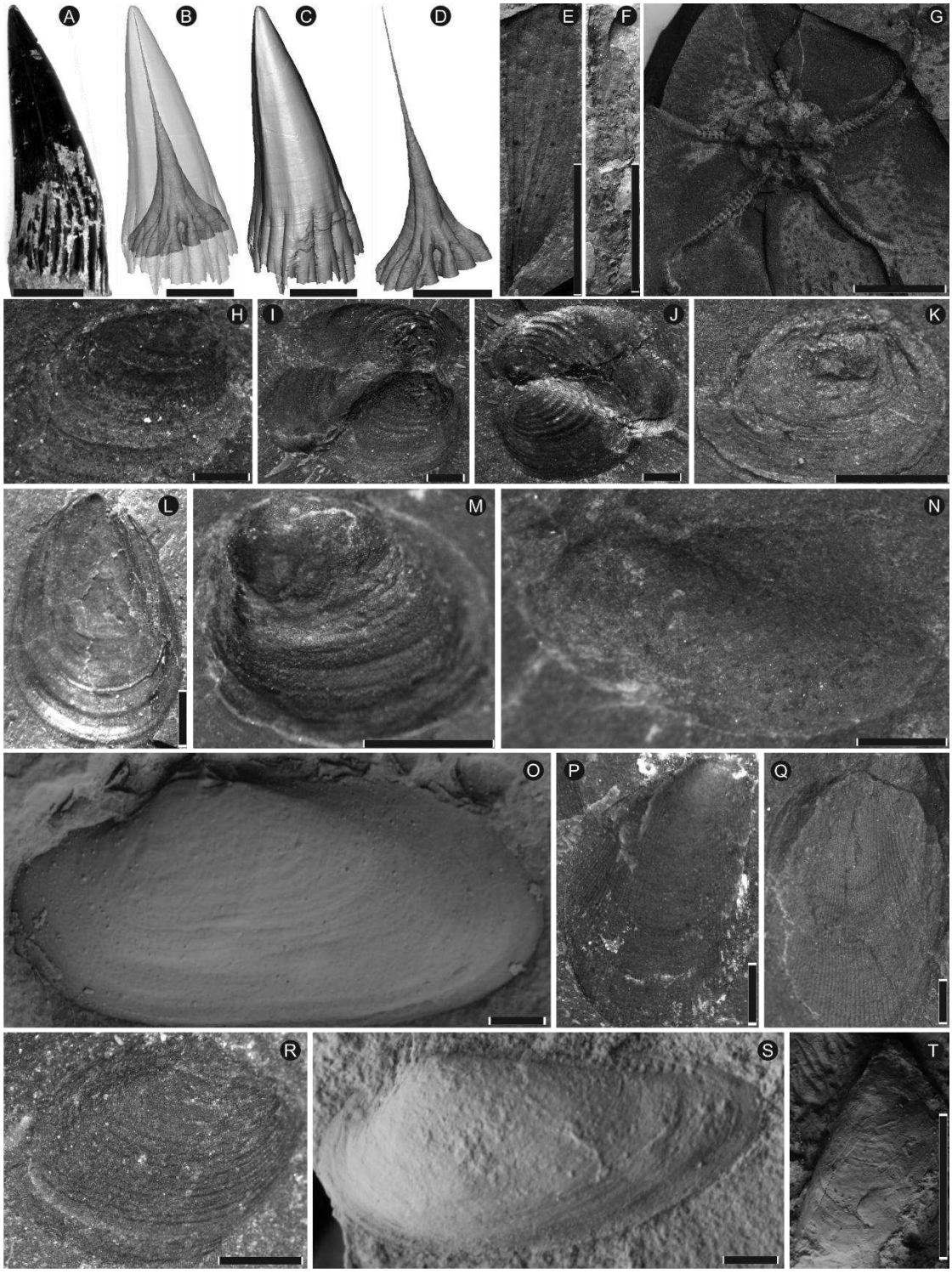

1234

1235 Figure 9

1236

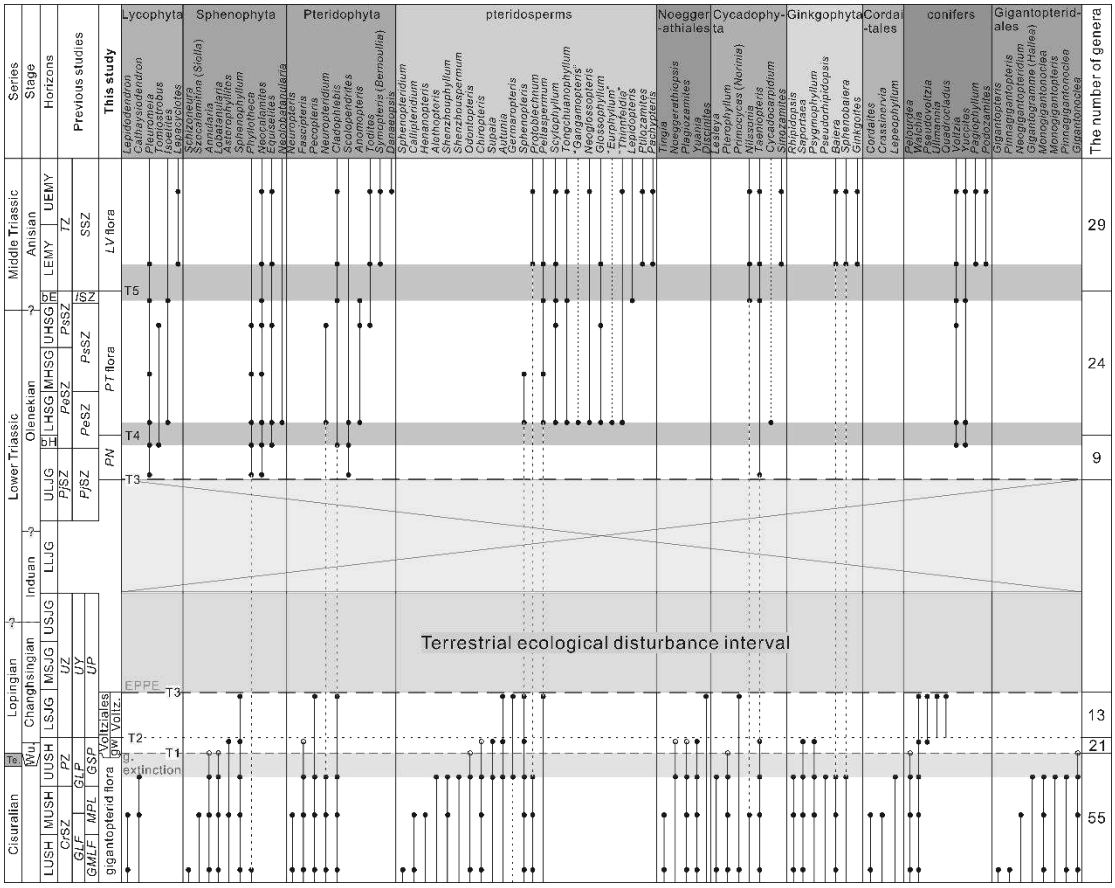

1237

1238 Figure 10

1239

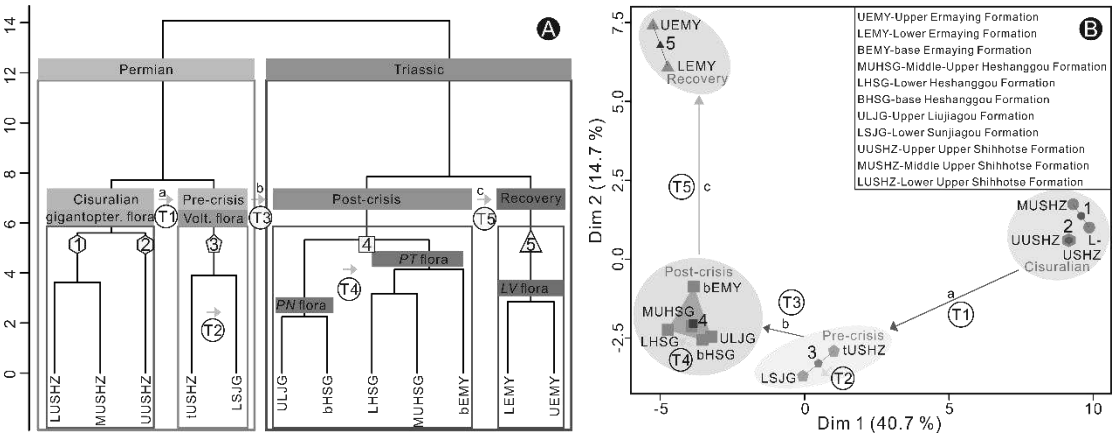

1240

1241 Figure 11

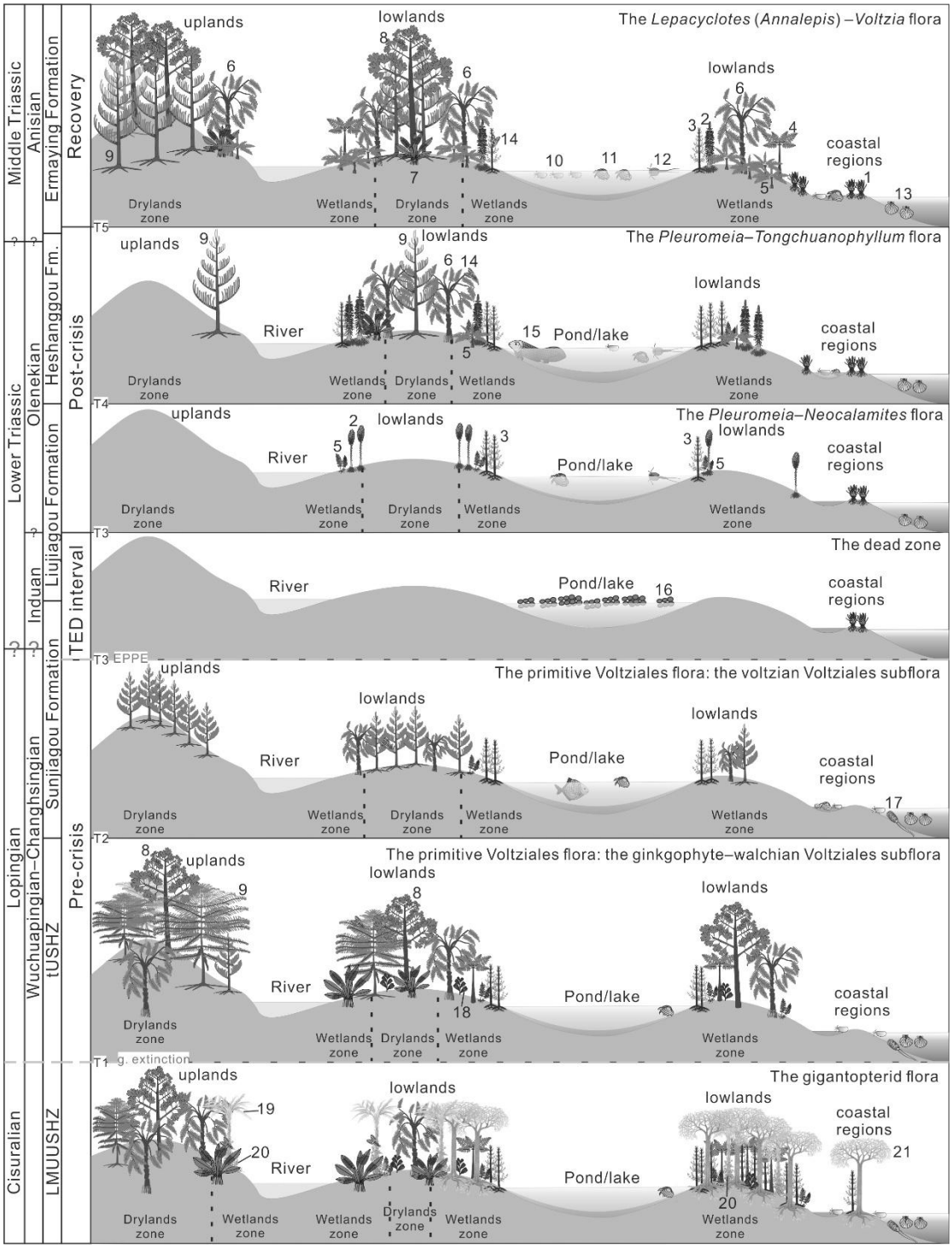

1242

1243 Figure 12

1244

1245

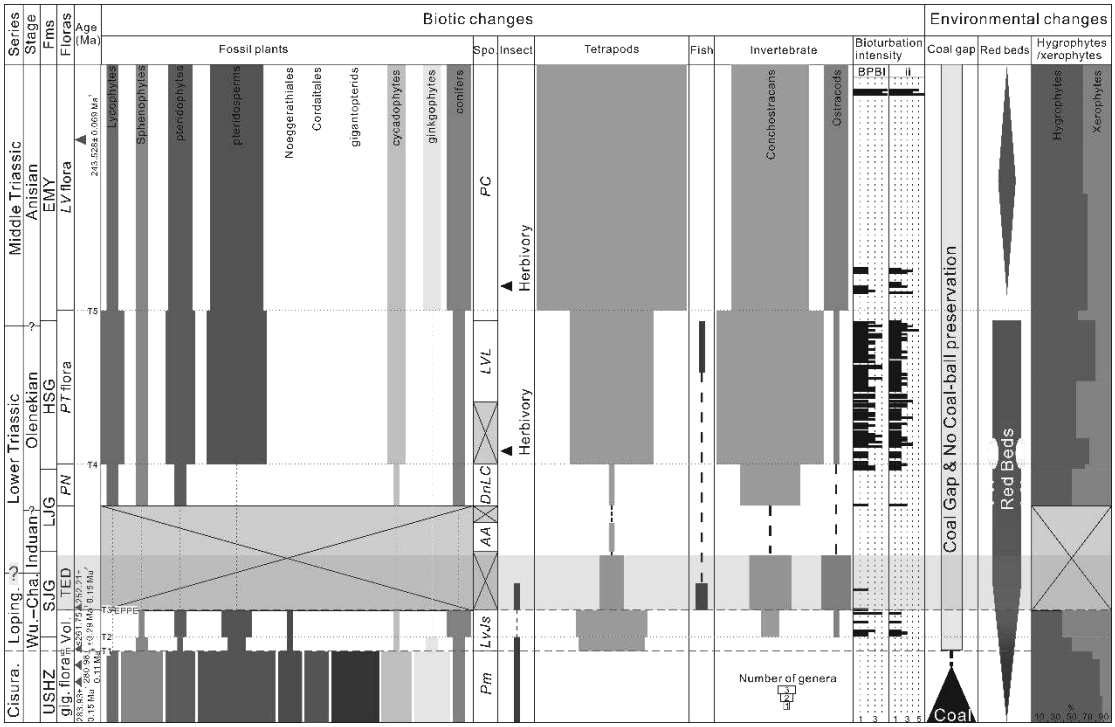

1246

1247 Figure 13